

Dimensionality reduction based on an overcomplete basis

Yoshinori Nakanishi-Ohno,^{1,2,*} Tomoyuki Obuchi,^{3,†}

Masato Okada,^{1,‡} and Yoshiyuki Kabashima^{3,§}

¹*Graduate School of Frontier Sciences,*

The University of Tokyo, Kashiwa, Chiba, 277-8561, Japan

²*Research Fellow of Japan Society for the Promotion*

of Science, Chiyoda, Tokyo, 102-0083, Japan

³*Interdisciplinary Graduate School of Science and Engineering,*

Tokyo Institute of Technology, Yokohama, Kanagawa, 226-8502, Japan

(Dated: January 18, 2019)

Abstract

We discuss a strategy of dimensionality reduction that is based on the use of an overcomplete basis, and evaluate its performance when a random matrix is used as this basis. A small combination of basis vectors is chosen from a given overcomplete basis, according to a given reduction rate, such that they compactly describe the target data with as small a reconstruction error as possible. As a selection method, we propose the ℓ_0 - and ℓ_1 -based methods, which employ the exhaustive search and ℓ_1 -norm regularization techniques, respectively. The performance is assessed in terms of the trade-off relation between the reconstruction error ϵ and the reduction rate r . First, we evaluate the performance analytically in the case that the methods are carried out ideally, using methods of statistical mechanics. The analytical result is then confirmed by performing numerical experiments on finite size systems, and extrapolating the results to the infinite-size limit. Our result provides a quantitative relation between the reconstruction error and the number of usable basis vectors, and clarifies the fact that the ℓ_0 -based method greatly outperforms the ℓ_1 -based one. An interesting outcome of our analysis is that any small value of error is achievable for any fixed reduction rate r in the large-size limit of the overcomplete basis, for both the ℓ_0 - and ℓ_1 -based methods. The difference between the two methods is manifested in the size of the overcomplete basis that is required in order to achieve the desired value for the reconstruction error $\hat{\epsilon}$. As $\hat{\epsilon}$ decreases, the required size grows in a polynomial and an exponential manners for the ℓ_0 - and ℓ_1 -based methods, respectively. Second, we examine the practical performances of two well-known algorithms, orthogonal matching pursuit and approximate message passing, when they are used to execute the ℓ_0 - and ℓ_1 -based methods, respectively. Our examination shows that orthogonal matching pursuit achieves a much better performance than the exact execution of the ℓ_1 -based method, as well as approximate message passing. However, regarding the ℓ_0 -based method, there is still room to design more effective greedy algorithms than orthogonal matching pursuit. Finally, we evaluate the performances of the algorithms when they are applied to image data compression.

* nakanishi@mns.k.u-tokyo.ac.jp

† obuchi@sp.dis.titech.ac.jp

‡ okada@k.u-tokyo.ac.jp

§ kaba@dis.titech.ac.jp

I. INTRODUCTION

Information processing based on the sparseness of various data is an active area of research. This sparseness means that data are typically expressed by a small combination of non-zero components when a proper basis is used. The significance of sparseness for information processing had already begun to be noted when principal component analysis was invented, in 1901 [1]. Low-rank approximation of a matrix is known to be a useful method of collaborative filtering for recommendation systems [2–4]. In neuroscience, the sparse-coding hypothesis has gradually been accepted as a method of elucidating visual and auditory systems [5–10]. Recent interest in information processing with sparse data has been triggered by compressed sensing, since it was demonstrated that ℓ_1 -norm minimization can give exact solutions in a reasonable time, under appropriate conditions [11–14].

In this study, we discuss sparse data processing from a different viewpoint, namely that of dimensionality reduction. Dimensionality reduction refers to the process of reducing the number of non-zero elements describing the target data, the purpose of which is to achieve a better trade-off relation between the reconstruction error and the reduction rate [15, 16]. We adopt a strategy of dimensionality reduction that utilizes an overcomplete basis (OCB). OCBs contain more basis vectors than the dimensionality of the target data. This means that a better and smaller set of basis vectors may be chosen to compactly express the data. Therefore, in terms of the trade-off relation, the OCB-based strategy is expected to outperform naive strategies such as random projection.

For selecting basis vectors from an overcomplete basis, we propose the ℓ_0 - and ℓ_1 -based methods, which employ the exhaustive search and ℓ_1 -norm regularization techniques, respectively. Our adoption of these methods is motivated by their application in compressed sensing [17]. Focusing on the trade-off relation, we evaluate the performance of dimensionality reduction from two different viewpoints. First, we analyze the theoretical performance that is achieved when the proposed methods are performed exactly, by using methods of statistical mechanics. We regard the reconstruction error and the reduction rate as the thermal averages of physical quantities derived from partition functions. In the large-system limit, these are assessed by the replica method and the saddle-point method [18, 19]. In order to validate the results of our analysis, we extrapolate physical quantities in the limit, from finite-size results obtained using the exchange Monte Carlo method [20] and quadratic

programming. Second, we investigate the practical performance of the OCB-based strategy. We examine the performances of two well-known algorithms, orthogonal matching pursuit [21, 22] and approximate message passing [23], when they are employed to approximately execute the ℓ_0 - and ℓ_1 -based methods, respectively. We also apply the approximate algorithms to a task of image data compression and evaluate their performances, as a practical example.

The rest of this paper is organized as follows. In Sec. II, we set up the problem that we will focus on, and introduce the ℓ_0 - and ℓ_1 -based methods. In Sec. III, we analyze the ideal performances of these methods, in terms of the trade-off relation. In Sec. IV, we discuss the practical performance of the OCB-based strategy, and its application to image data. In Sec. V, we conclude this paper.

II. PROBLEM SETTING

A. Dimensionality reduction using a random basis

Given a data vector $\mathbf{y} \in \mathbb{R}^M$ and a reduction rate r , the purpose of dimensionality reduction is to obtain a reduced vector $\mathbf{x} \in \mathbb{R}^N$ using a basis matrix $\mathbf{A} = (\mathbf{a}_1, \dots, \mathbf{a}_N) \in \mathbb{R}^{M \times N}$, while keeping the reconstruction error ϵ as small as possible. The reduction rate r is defined as the ratio of the number of non-zero components of \mathbf{x} to the dimension of the data vector. That is,

$$r = \frac{\|\mathbf{x}\|_0}{M}, \quad (1)$$

where $\|\cdot\|_0$ denotes the so-called ℓ_0 -norm of a vector. The ℓ_0 -norm represents the number of non-zero elements of a vector, defined as $\|\mathbf{v}\|_0 = \sum_i |v_i|_0$, where $|v_i|_0$ is equal to 0 ($v_i = 0$) or 1 ($v_i \neq 0$). We measure the reconstruction error using the mean squared error, as

$$\epsilon = \frac{1}{2M} \|\mathbf{y} - \mathbf{A}\mathbf{x}\|_2^2, \quad (2)$$

where $\|\cdot\|_2$ is the ℓ_2 -norm of a vector, defined as $\|\mathbf{v}\|_2 = \sqrt{\sum_i v_i^2}$. For our purpose of an analytical evaluation of ϵ , we consider the case where the elements of the data vector \mathbf{y} are independently and identically distributed (i.i.d.) random variables from the normal distribution, whose mean and variance are 0 and σ_y^2 , respectively, and together are denoted by $\mathcal{N}(0, \sigma_y^2)$. The elements of the basis matrix \mathbf{A} are also i.i.d. random variables from

$\mathcal{N}(0, M^{-1})$. Then, the matrix \mathbf{A} is almost surely of rank $\min(M, N)$, and the reconstruction error becomes a random variable.

If $N = rM$, the minimization of Eq. (2) involves nothing but the random projection of \mathbf{y} by \mathbf{A} , and the corresponding reduced vector is easily obtained as

$$\hat{\mathbf{x}} = \mathbf{A}^+ \mathbf{y}, \quad (3)$$

where \mathbf{A}^+ is the pseudoinverse (PI) of \mathbf{A} , given by

$$\mathbf{A}^+ = (\mathbf{A}^T \mathbf{A})^{-1} \mathbf{A}^T. \quad (4)$$

Let us call this the naive method, which is illustrated in Fig. 1(a). In the large-size limit $M \rightarrow \infty$, the corresponding error converges to

$$\epsilon_{\text{naive}} = \frac{1-r}{2} \sigma_y^2, \quad (5)$$

with probability one. In general, in the limit $M \rightarrow \infty$ certain random variables, such as ϵ , have the so-called self-averaging property, and will almost surely converge to their average values. This enables us to present a clear discussion, and hereafter we focus on this limit.

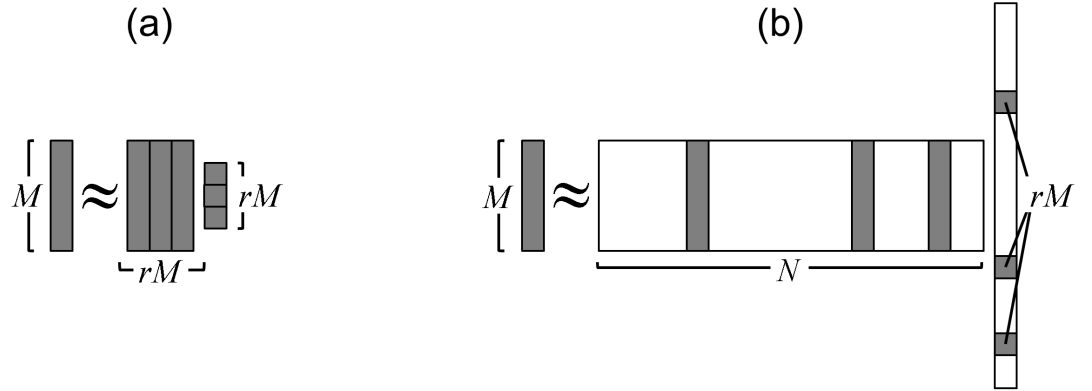


FIG. 1. Schematic diagrams of dimensionality reduction. (a) Naive method. (b) OCB-based strategy.

On the other hand, for $N > rM$ we have some options in choosing a combination of rM basis vectors from the matrix, as illustrated in Fig. 1(b). If the chosen combination is more suitable for representing the data vector than one that is chosen randomly, then the reconstruction error becomes smaller than ϵ_{naive} . This is the idea behind the OCB-based strategy. However, this strategy presents the problem of how to choose the combination of basis vectors. Our proposed methods, the ℓ_0 - and ℓ_1 -based methods, provide solutions to this problem.

B. Methods

1. ℓ_0 -based method

The basic idea of the ℓ_0 -based method is to minimize the reconstruction error by choosing the best combination of rM basis (column) vectors from a given OCB. More generally, we would like to define the reconstruction error as a function of the chosen combination of basis vectors, and to control it in a simple manner. This motivates us to introduce a binary vector $\mathbf{c} \in \{1, 0\}^N$, to store information on whether each basis vector is chosen ($c_i = 1$) or not ($c_i = 0$). We also introduce a reconstruction error, labelled by \mathbf{c} , with

$$\epsilon(\mathbf{c}|\mathbf{y}, \mathbf{A}) = \min_{\mathbf{x}} \left\{ \frac{1}{2M} \|\mathbf{y} - \mathbf{A}(\mathbf{c} \circ \mathbf{x})\|_2^2 \right\}, \quad (6)$$

where \circ is the Hadamard product of two vectors, defined as $(\mathbf{v} \circ \mathbf{w})_i = v_i w_i$. In addition, we define an entropy function $s(\epsilon|\mathbf{y}, \mathbf{A})$ to represent the number of configurations \mathbf{c} that give a value of ϵ for the reconstruction error, as follows:

$$s(\epsilon|\mathbf{y}, \mathbf{A}) = \frac{1}{M} \ln (\#\{\mathbf{c} \mid \|\mathbf{c}\|_0 = rM \wedge \epsilon(\mathbf{c}|\mathbf{y}, \mathbf{A}) = \epsilon\}), \quad (7)$$

where $\#$ denotes the number of elements of the following set.

This entropy function is expected to be analytic and convex upward with respect to ϵ , and cannot be negative, by definition. A typical shape of the entropy is depicted in Fig. 2. The smaller zero point ϵ_0 of the entropy function, $s(\epsilon_0) = 0$, gives the minimum value of the

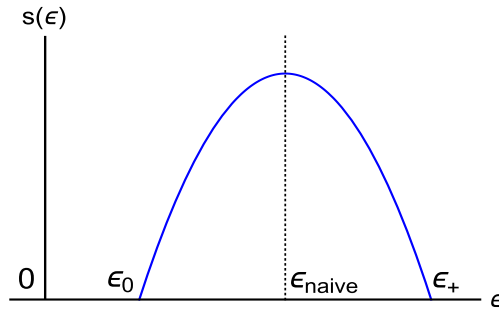


FIG. 2. A schematic shape of the entropy function. The smaller zero point of the entropy, ϵ_0 , corresponds to the minimum of the reconstruction error connected to the best combination of the basis vectors, and the point giving the largest entropy value is ϵ_{naive} .

reconstruction error

$$\epsilon_0(\mathbf{y}, \mathbf{A}) = \min_{\mathbf{c}} \epsilon(\mathbf{c}|\mathbf{y}, \mathbf{A}) \quad \text{subj. to } \|\mathbf{c}\|_0 = rM. \quad (8)$$

Hence, our original motivation for introducing the ℓ_0 -based method, to find the minimum reconstruction error led by the best combination of basis vectors, can be achieved through the evaluation of the entropy function. In addition, the evaluation of the entropy function is easier than the direct evaluation of ϵ_0 , and moreover the entropy function provides more information about the space of the variables \mathbf{c} , which can be useful for practical applications such as designing algorithms. Thus, the entropy function $s(\epsilon)$ is the primary object of our analysis in the ℓ_0 -based method. A similar analysis has been proposed for examining the weight space structure of multilayer perceptrons [24].

2. ℓ_1 -based method

The ℓ_0 -based method is the most closely matched to the original idea of the OCB-based strategy. However, its algorithmic realization of searching combinations of basis vectors is computationally inefficient, because it requires an exponentially growing computational cost as the system size N increases. In practical situations, instead of the ℓ_0 -based method, a method based on ℓ_1 -norm regularization can be employed. This motivates us to propose and examine the following ℓ_1 -based method.

Our ℓ_1 -based method arises from the following minimization problem:

$$\hat{\boldsymbol{\xi}} = \arg \min_{\boldsymbol{\xi}} \left\{ \frac{1}{2} \|\mathbf{y} - \mathbf{A}\boldsymbol{\xi}\|_2^2 + \lambda \|\boldsymbol{\xi}\|_1 \right\}, \quad (9)$$

where $\|\cdot\|_1$ is the ℓ_1 -norm of a vector, defined as $\|\mathbf{v}\|_1 = \sum_i |v_i|$, with the absolute value denoted by $|\cdot|$. The solution of this minimization problem, $\hat{\boldsymbol{\xi}}$, provides useful information for finding the reduced vector we desire. This minimization problem is equivalent to the least absolute shrinkage and selection operator, also known as LASSO [25]. The main benefit of this approach (9) is the computational ease of performing the minimization. As the objective function of (9) is convex, its minimization can be exactly carried out with a computational time in $O(N^3)$, using versatile algorithms. Furthermore, the ℓ_1 -norm term in Eq. (9) results in a sparsifying effect in $\hat{\boldsymbol{\xi}}$, and its coefficient λ is adjusted according to the reduction rate. Namely, λ is chosen so that $\|\hat{\boldsymbol{\xi}}\|_0 = rM$.

Our aim in the analysis in the ℓ_1 -case is to evaluate the reconstruction error resulting from $\hat{\boldsymbol{\xi}}$. The expression of the reconstruction error is given by

$$\epsilon_1 = \frac{1}{2M} \|\mathbf{y} - \mathbf{A}\hat{\boldsymbol{\xi}}\|_2^2. \quad (10)$$

An inconvenience presented by this error is that it is not minimized on the set of basis vectors chosen by $\hat{\boldsymbol{\xi}}$, owing to the presence of the ℓ_1 -norm term. In order to remove this extra error, we propose that after determining the positions of the non-zero elements of the reduced vector determined by $\hat{\boldsymbol{\xi}}$, the values of the non-zero components are determined again by purely minimizing the reconstruction error. This procedure is described as follows:

$$\epsilon_1^{\text{PI}} = \min_{\mathbf{x}} \left\{ \frac{1}{2M} \|\mathbf{y} - \mathbf{A}(|\hat{\boldsymbol{\xi}}|_0 \circ \mathbf{x})\|_2^2 \right\}, \quad (11)$$

where $|\cdot|_0$ of a vector is defined by $(|\mathbf{v}|_0)_i = |v_i|_0$. This can be carried out easily by the PI operation for the sub-matrix of \mathbf{A} that is composed of columns corresponding to $|\hat{\xi}_i|_0 = 1$. These two quantities, ϵ_1 and ϵ_1^{PI} , are the objects of our analysis in the ℓ_1 case.

III. ANALYSIS OF IDEAL PERFORMANCE

A. Analytical treatment in the limit $M \rightarrow \infty$

We investigate the limit $M \rightarrow \infty$, as stated above. For this purpose, we employ some statistical mechanical tools, which provide useful assistance investigating this limit. According to the terminology of statistical mechanics, we call the limit $M \rightarrow \infty$ the thermodynamic limit, and the average over \mathbf{y} and \mathbf{A} the configurational average, which is denoted by $[\cdot]_{\mathbf{y}, \mathbf{A}}$. In taking the limit $M \rightarrow \infty$, the aspect ratio of the basis matrix, $\alpha = M/N$, is fixed.

1. ℓ_0 -based method

A versatile technique of statistical mechanics is to introduce a generating function Z of an energy function \mathcal{H} , called a partition function. This defines a canonical distribution p . In the ℓ_0 case, we define the energy function, partition function, and canonical distribution

respectively as follows:

$$\mathcal{H}_0(\mathbf{c}; \beta | \mathbf{y}, \mathbf{A}) = -\frac{1}{\beta} \ln \int d_{\mathbf{c}} \mathbf{x} e^{-\frac{\beta}{2} \|\mathbf{y} - \mathbf{A}(\mathbf{c} \odot \mathbf{x})\|_2^2}, \quad (12)$$

$$Z_0(\mu, \beta | \mathbf{y}, \mathbf{A}) = \sum_{\mathbf{c}} \delta(Mr - \|\mathbf{c}\|_0) e^{-\mu \mathcal{H}_0(\mathbf{c}; \beta | \mathbf{y}, \mathbf{A})} \equiv \text{Tr}_{\mathbf{c}} e^{-\mu \mathcal{H}_0(\mathbf{c}; \beta | \mathbf{y}, \mathbf{A})}, \quad (13)$$

$$p_0(\mathbf{c}; \mu, \beta | \mathbf{y}, \mathbf{A}) = \frac{1}{Z_0(\mu, \beta | \mathbf{y}, \mathbf{A})} \delta(Mr - \|\mathbf{c}\|_0) e^{-\mu \mathcal{H}_0(\mathbf{c}; \beta | \mathbf{y}, \mathbf{A})}, \quad (14)$$

where $\int d_{\mathbf{c}} x_i$ is equal to $\int dx_i$ ($c_i = 1$) or 1 ($c_i = 0$). This energy function is related to the reconstruction error of a given basis-vector choice \mathbf{c} as follows:

$$\frac{1}{M} \lim_{\beta \rightarrow \infty} \mathcal{H}_0(\mathbf{c}; \beta | \mathbf{y}, \mathbf{A}) = \epsilon(\mathbf{c} | \mathbf{y}, \mathbf{A}). \quad (15)$$

The cumulant generating function $\phi_0(\mu | \mathbf{y}, \mathbf{A})$ is obtained from Z_0 by

$$\phi_0(\mu | \mathbf{y}, \mathbf{A}) = \lim_{\beta \rightarrow \infty} \frac{1}{M} \ln Z_0(\mu, \beta | \mathbf{y}, \mathbf{A}), \quad (16)$$

and is connected to the entropy (7) by the Legendre transformation in the large M limit, as

$$\phi_0(\mu | \mathbf{y}, \mathbf{A}) = \max_{\epsilon_0 \leq \epsilon \leq \epsilon_+} \{s(\epsilon | \mathbf{y}, \mathbf{A}) - \mu \epsilon\}. \quad (17)$$

The maximization problem of Eq. (17) must be solved on the well-defined region of s , which requires appropriate bounds ϵ_0 and ϵ_+ . Overall, we can calculate the object of our analysis, $s(\epsilon)$, through the inverse Legendre transformation, once we have obtained ϕ_0 . Therefore, we turn our attention to the calculation of ϕ_0 .

The cumulant-generating function has the self-averaging property, as does the entropy, and we assess the configurational average, given by

$$\phi_0(\mu) = [\phi_0(\mu | \mathbf{y}, \mathbf{A})]_{\mathbf{y}, \mathbf{A}}. \quad (18)$$

We employ the replica method in order to calculate this average, and a detailed analysis is provided in Appendix A. The result is given by

$$\begin{aligned} \phi_0(\mu) = \text{extr}_{\hat{\Theta}_0} & \left\{ \frac{1}{2} \ln \frac{1 + \chi}{1 + \chi + \mu(Q - q)} - \frac{1}{2} \frac{\mu(q + \sigma_y^2)}{1 + \chi + \mu(Q - q)} \right. \\ & \left. + \frac{1}{2} \left(\hat{r}r + \hat{Q}Q - \frac{\hat{\chi}}{\mu} \chi + \hat{q}q \right) + \frac{1}{\alpha} \int Dz \ln(1 + Y) \right\}, \end{aligned} \quad (19)$$

where $\text{extr}_{\hat{\Theta}}\{\cdot\}$ denotes the operation of extremization with respect to Θ , $\hat{\Theta}_0 = \{Q, \chi, q, \hat{r}, \hat{Q}, \hat{\chi}, \hat{q}\}$, and $\int Dz = \int \frac{dz}{\sqrt{2\pi}} e^{-\frac{z^2}{2}}$, and we set

$$Y \equiv \sqrt{\frac{\hat{\chi} + \hat{Q}}{\hat{Q} + \hat{q}}} e^{-\frac{1}{2}\hat{r} + \frac{1}{2}\frac{\hat{q}}{\hat{Q} + \hat{q}} z^2}. \quad (20)$$

By applying the extremization condition, we obtain the following equations of state (EOSs):

$$\hat{\chi} = \mu^2 \left\{ \frac{\Delta}{(1+\chi)(1+\chi+\mu\Delta)} + \frac{\sigma_y^2 + q}{(1+\chi+\mu\Delta)^2} \right\}, \quad (21a)$$

$$\hat{Q} = \mu \left\{ \frac{1}{1+\chi+\mu\Delta} - \frac{\mu(\sigma_y^2 + q)}{(1+\chi+\mu\Delta)^2} \right\}, \quad (21b)$$

$$\hat{q} = \mu^2 \frac{\sigma_y^2 + q}{(1+\chi+\mu\Delta)^2}, \quad (21c)$$

$$r = \frac{1}{\alpha} \int Dz \frac{Y}{1+Y}, \quad (21d)$$

$$\chi = \frac{\mu r}{\hat{\chi} + \hat{Q}}, \quad (21e)$$

$$Q = r \frac{\hat{\chi} - \hat{q}}{(\hat{\chi} + \hat{Q})(\hat{Q} + \hat{q})} + \frac{1}{\alpha} \frac{\hat{q}}{(\hat{Q} + \hat{q})^2} \int Dz z^2 \frac{Y}{1+Y}, \quad (21f)$$

$$q = \frac{1}{\alpha} \frac{\hat{q}}{(\hat{Q} + \hat{q})^2} \int Dz z^2 \left(\frac{Y}{1+Y} \right)^2. \quad (21g)$$

where we write $\Delta = Q - q$. From the EOSs, we obtain some simple and general relations, which we summarize here for later convenience:

$$\hat{\chi} + \hat{Q} = \frac{\mu}{1+\chi}, \quad (22a)$$

$$\hat{Q} + \hat{q} = \frac{\mu}{1+\chi+\mu\Delta}, \quad (22b)$$

$$\hat{\chi} - \hat{q} = \frac{\mu^2 \Delta}{(1+\chi)(1+\chi+\mu\Delta)}, \quad (22c)$$

$$\chi = \frac{r}{1-r}. \quad (22d)$$

The relation involving the entropy, Eq. (17), enables us to employ a convenient parametric form of $\epsilon(\mu)$ and $s(\mu) = s(\epsilon(\mu))$, and Eqs. (21,22) allow us to simplify $\epsilon(\mu)$, as

$$\epsilon(\mu) = -\frac{\partial \phi_0(\mu)}{\partial \mu} = \frac{\hat{\chi}}{2\mu^2}, \quad (23)$$

$$s(\mu) = \phi_0(\mu) + \mu \epsilon(\mu). \quad (24)$$

The explicit form of $s(\mu)$ is not enlightening, and therefore we omit it.

Here, we make a technical remark on the derivation of Eq. (19). In contrast to the usual prescription of the replica method, we require two different replica numbers for the present analysis, because we have two different integration variables, \mathbf{x} and \mathbf{c} , in the calculation of

ϕ_0 . Using Eqs. (16,18) and introducing a variable $\nu = \mu/\beta$, we can rewrite $\phi_0(\mu)$ as

$$\begin{aligned}\phi_0(\mu) &= \lim_{\nu \rightarrow 0} \frac{1}{M} \left[\ln \text{Tr}_{\mathbf{c}} \left(\int d\mathbf{c} \mathbf{x} e^{-\frac{1}{2} \frac{\mu}{\nu} \|\mathbf{y} - \mathbf{A}(\mathbf{c} \circ \mathbf{x})\|_2^2} \right)^\nu \right]_{\mathbf{y}, \mathbf{A}} \\ &= \lim_{n \rightarrow 0} \lim_{\nu \rightarrow 0} \frac{1}{Mn} \ln \left[\left\{ \text{Tr}_{\mathbf{c}} \left(\int d\mathbf{c} \mathbf{x} e^{-\frac{1}{2} \frac{\mu}{\nu} \|\mathbf{y} - \mathbf{A}(\mathbf{c} \circ \mathbf{x})\|_2^2} \right)^\nu \right\}^n \right]_{\mathbf{y}, \mathbf{A}}.\end{aligned}\quad (25)$$

In the last line, we use the replica identity $[\ln X]_{\mathbf{y}, \mathbf{A}} = \lim_{n \rightarrow 0} (1/n) \ln [X^n]_{\mathbf{y}, \mathbf{A}}$. We identify n and ν as the two replica numbers, and assume that they are natural numbers, which enables us to expand the powers and to calculate the configurational average. The remaining calculations follow the usual procedure of the replica method, and we assume the replica symmetry (RS) ansatz in the order parameters [26]. The RS assumption will be justified later, in a comparison with numerical calculations.

2. ℓ_1 -based method

a. Derivation of ϵ_1 Similarly to the case of the ℓ_0 -based method, the energy function, partition function, and canonical distribution of the ℓ_1 case are defined respectively as

$$\mathcal{H}_1(\boldsymbol{\xi} | \mathbf{y}, \mathbf{A}) = \frac{1}{2} \|\mathbf{y} - \mathbf{A}\boldsymbol{\xi}\|_2^2 + \lambda \|\boldsymbol{\xi}\|_1, \quad (26)$$

$$Z_1(\mu, \kappa | \mathbf{y}, \mathbf{A}) = \int d\boldsymbol{\xi} e^{-\mu(\mathcal{H}_1(\boldsymbol{\xi} | \mathbf{y}, \mathbf{A}) + \kappa \|\boldsymbol{\xi}\|_0)}, \quad (27)$$

$$p_1(\boldsymbol{\xi}; \mu, \kappa | \mathbf{y}, \mathbf{A}) = \frac{1}{Z_1(\mu, \kappa | \mathbf{y}, \mathbf{A})} e^{-\mu(\mathcal{H}_1(\boldsymbol{\xi} | \mathbf{y}, \mathbf{A}) + \kappa \|\boldsymbol{\xi}\|_0)}. \quad (28)$$

The energy function \mathcal{H}_1 is exactly the minimized object in Eq. (9). We also introduce the averaged free-energy density, given by

$$f_1(\mu, \kappa) = -\frac{1}{M\mu} [\ln Z_1(\mu, \kappa | \mathbf{y}, \mathbf{A})]_{\mathbf{y}, \mathbf{A}}, \quad (29)$$

which plays the role of the cumulant-generating function that is given by ϕ_0 in the ℓ_0 case. In the limit $\mu \rightarrow \infty$, the minimizer of the energy function becomes dominant in p_1 , and we focus on this limit. Any quantity of interest can be calculated from f_1 . For example, the reduction rate r and the reconstruction error ϵ_1 are calculated as

$$r = \lim_{\mu \rightarrow \infty} \lim_{\kappa \rightarrow 0} \frac{\partial}{\partial \kappa} f_1(\mu, \kappa), \quad (30)$$

$$\epsilon_1 = \lim_{\mu \rightarrow \infty} \left(1 + \mu \frac{\partial}{\partial \mu} - \lambda \frac{\partial}{\partial \lambda} \right) f_1(\mu, 0). \quad (31)$$

An analytically compact form of f_1 is assessed by using the replica method in the limit $M \rightarrow \infty$, through the replica identity, as

$$f_1(\mu, \kappa) = -\lim_{n \rightarrow 0} \frac{1}{M\mu n} \ln [Z_1^n(\mu, \kappa | \mathbf{y}, \mathbf{A})]_{\mathbf{y}, \mathbf{A}}. \quad (32)$$

As in the ℓ_0 case, we assume the RS solution. The details of the necessary calculations are presented in Appendix B. The result is given by

$$f_1(\mu \rightarrow \infty, \kappa) = \text{extr}_{\hat{\Theta}_1} \left\{ \frac{1}{2} \frac{P + \sigma_y^2}{1 + \chi_p} - \frac{1}{2} (\hat{P}P - \hat{\chi}_p \chi_p) - \frac{\hat{\chi}_p}{2\alpha\hat{P}} \left((1 + 2\theta_+\theta_-) \text{erfc}(\theta_+) - \theta_- \frac{2}{\sqrt{\pi}} e^{-\theta_+^2} \right) \right\}, \quad (33)$$

where $\hat{\Theta}_1 = \{P, \chi_p, \hat{P}, \hat{\chi}_p\}$, $\theta_{\pm} = \frac{\lambda \pm \sqrt{2\kappa\hat{P}}}{\sqrt{2\hat{\chi}_p}}$, and $\text{erfc}(\cdot)$ is the complementary error function, defined as $\text{erfc}(x) = \frac{2}{\sqrt{\pi}} \int_x^\infty dt e^{-t^2}$. The extremization condition gives the following EOSs for the present case:

$$\hat{\chi}_p = \frac{P + \sigma_y^2}{(1 + \chi_p)^2}, \quad (34a)$$

$$\hat{P} = \frac{1}{1 + \chi_p}, \quad (34b)$$

$$\chi_p = \frac{1}{\alpha\hat{P}} \left(\text{erfc}(\theta_+) + \sqrt{\frac{\kappa\hat{P}}{\hat{\chi}_p}} \frac{2}{\sqrt{\pi}} e^{-\theta_+^2} \right), \quad (34c)$$

$$P = \frac{\hat{\chi}_p}{\alpha\hat{P}^2} \left((1 + 2\theta_+\theta_-) \text{erfc}(\theta_+) - \theta_- \frac{2}{\sqrt{\pi}} e^{-\theta_+^2} \right) + \frac{\kappa}{\alpha\hat{P}} \text{erfc}(\theta_+). \quad (34d)$$

By using Eqs. (30,31), we obtain

$$r = \frac{1}{\alpha} \text{erfc}(\theta) \quad (35)$$

$$\epsilon_1 = \frac{1}{2} \frac{P + \sigma_y^2}{1 + \chi_p} - \frac{1}{2} (\hat{P}P - \hat{\chi}_p \chi_p) - \frac{\hat{\chi}_p}{2\alpha\hat{P}} \left((1 - 2\theta^2) \text{erfc}(\theta) + \theta \frac{2}{\sqrt{\pi}} e^{-\theta^2} \right), \quad (36)$$

where $\theta = \frac{\lambda}{\sqrt{2\hat{\chi}_p}}$. In addition, a simple formula

$$\epsilon_1 = \frac{1}{2} \hat{\chi}_p. \quad (37)$$

is derived from the EOSs of Eq. (34) in the limit $\kappa \rightarrow 0$, and a useful relation

$$\chi_p = \frac{r}{1 - r}, \quad (38)$$

which is similar to Eq. (22d), is offered by Eqs. (34,35).

b. Derivation of ϵ_1^{PI} We also evaluate ϵ_1^{PI} , as defined in Eq. (11). The computations are rather technical, and there we defer the details to Appendix B. Here, we present an outline of the analysis, and the result.

Again, we use the energy function defined in the ℓ_0 case, but here the argument is $|\boldsymbol{\xi}|_0$, determined by $p_1(\boldsymbol{\xi})$. Thus, we obtain

$$\mathcal{H}_0(|\boldsymbol{\xi}|_0; \beta | \mathbf{y}, \mathbf{A}) = -\frac{1}{\beta} \ln \int d|\boldsymbol{\xi}|_0 \mathbf{x} e^{-\frac{\beta}{2} \|\mathbf{y} - \mathbf{A}(|\boldsymbol{\xi}|_0 \odot \mathbf{x})\|_2^2}. \quad (39)$$

Since the vector $\boldsymbol{\xi}$ is drawn from p_1 , we calculate the average value of $(1/M)\mathcal{H}_0(|\boldsymbol{\xi}|_0)$ over p_1 , in addition to the configurational average. Taking the limits $\beta \rightarrow \infty$ and $\mu \rightarrow \infty$, we obtain the desired reconstruction error ϵ_1^{PI} . For simplicity of analysis, we set $\mu = \beta$, and take both limits to infinity simultaneously. Thus, we have

$$\epsilon_1^{\text{PI}} = \lim_{\mu \rightarrow \infty} \frac{1}{M} \left[\int d\boldsymbol{\xi} p_1(\boldsymbol{\xi}; \mu, 0 | \mathbf{y}, \mathbf{A}) \mathcal{H}_0(|\boldsymbol{\xi}|_0; \mu | \mathbf{y}, \mathbf{A}) \right]_{\mathbf{y}, \mathbf{A}}. \quad (40)$$

By utilizing the replica method again, we can calculate this. We defer the details of the calculations to Appendix B, and here write down the resultant formula:

$$\begin{aligned} \epsilon_1^{\text{PI}} = \text{extr}_{\hat{\Theta}_1^{\text{PI}}} & \left\{ \frac{1}{2} \frac{P + \sigma_y^2}{1 + \chi_q} \left(\frac{\chi_c}{1 + \chi_p} \right)^2 - \frac{C + \sigma_y^2}{1 + \chi_q} \frac{\chi_c}{1 + \chi_p} + \frac{1}{2} \frac{Q + \sigma_y^2}{1 + \chi_q} \right. \\ & - (\hat{C}C - \hat{\chi}_c \chi_c) - \frac{1}{2} (\hat{Q}Q - \hat{\chi}_q \chi_q) \\ & \left. - \frac{\hat{\chi}_p}{2\alpha \hat{Q}} \left(\left(\frac{\hat{\chi}_q}{\hat{\chi}_p} - 2 \frac{\hat{\chi}_c}{\hat{\chi}_p} \frac{\hat{C}}{\hat{P}} + (1 + 2\theta^2) \frac{\hat{C}^2}{\hat{P}^2} \right) \text{erfc}(\theta) + \theta \left(\frac{\hat{\chi}_c^2}{\hat{\chi}_p^2} - \frac{\hat{C}^2}{\hat{P}^2} \right) \frac{2}{\sqrt{\pi}} e^{-\theta^2} \right) \right\}, \quad (41) \end{aligned}$$

where $\hat{\Theta}_1^{\text{PI}} = \{C, \chi_c, Q, \chi_q, \hat{C}, \hat{\chi}_c, \hat{Q}, \hat{\chi}_q\}$, and $\theta = \frac{\lambda}{\sqrt{2\hat{\chi}_p}}$. One point to remark on is that we should not take the extremization condition with respect to $\hat{\Theta}_1 = \{P, \chi_p, \hat{P}, \hat{\chi}_p\}$ in this expression. Instead, we should substitute the extremizer of (33) into it. Applying the

extremization condition with respect to $\hat{\Theta}^{\text{PI}}$ gives

$$\hat{\chi}_q = \frac{P + \sigma_y^2}{(1 + \chi_q)^2} \left(\frac{\chi_c}{1 + \chi_p} \right)^2 - 2 \frac{C + \sigma_y^2}{(1 + \chi_q)^2} \frac{\chi_c}{1 + \chi_p} + \frac{Q + \sigma_y^2}{(1 + \chi_q)^2}, \quad (42a)$$

$$\hat{Q} = \frac{1}{1 + \chi_q}, \quad (42b)$$

$$\hat{\chi}_c = -\frac{P + \sigma_y^2}{1 + \chi_q} \frac{\chi_c}{(1 + \chi_p)^2} + \frac{C + \sigma_y^2}{1 + \chi_q} \frac{1}{1 + \chi_p} \quad (42c)$$

$$\hat{C} = -\frac{1}{1 + \chi_q} \frac{\chi_c}{1 + \chi_p}, \quad (42d)$$

$$\chi_q = \frac{1}{\alpha \hat{Q}} \text{erfc}(\theta), \quad (42e)$$

$$Q = \frac{\hat{\chi}_p}{\alpha \hat{Q}^2} \left(\left(\frac{\hat{\chi}_q}{\hat{\chi}_p} - 2 \frac{\hat{\chi}_c}{\hat{\chi}_p} \frac{\hat{C}}{\hat{P}} + (1 + 2\theta^2) \frac{\hat{C}^2}{\hat{P}^2} \right) \text{erfc}(\theta) + \theta \left(\frac{\hat{\chi}_c^2}{\hat{\chi}_p^2} - \frac{\hat{C}^2}{\hat{P}^2} \right) \frac{2}{\sqrt{\pi}} e^{-\theta^2} \right), \quad (42f)$$

$$\chi_c = \frac{1}{\alpha \hat{Q}} \left(-\frac{\hat{C}}{\hat{P}} \text{erfc}(\theta) + \theta \frac{\hat{\chi}_c}{\hat{\chi}_p} \frac{2}{\sqrt{\pi}} e^{-\theta^2} \right), \quad (42g)$$

$$C = -\frac{\hat{\chi}_p}{\alpha \hat{Q}} \left(\left(-\frac{\hat{\chi}_c}{\hat{\chi}_p} \frac{1}{\hat{P}} + (1 + 2\theta^2) \frac{\hat{C}}{\hat{P}^2} \right) \text{erfc}(\theta) - \theta \frac{\hat{C}}{\hat{P}^2} \frac{2}{\sqrt{\pi}} e^{-\theta^2} \right). \quad (42h)$$

From the EOSs, we can obtain the following simple relations:

$$\chi_q = \frac{r}{1 - r} = \chi_p, \quad (43a)$$

$$\hat{Q} = \hat{P} = \frac{1}{1 + \chi_p}, \quad (43b)$$

$$\epsilon_1^{\text{PI}} = \frac{1}{2} \hat{\chi}_q. \quad (43c)$$

We now make some comments regarding the derivation of Eq. (41). In order to calculate the configurational average, we are required to deal with two different factors, Z_1 in $p_1 = (1/Z_1)e^{-\mu\mathcal{H}_1}$, and the logarithm in \mathcal{H}_0 . Correspondingly, as in the ℓ_0 case, we introduce replicas of two different kinds: n replicas to handle $1/Z_1$, and ν replicas to handle the logarithm. Using them, we can rewrite Eq. (40) as

$$\epsilon_1^{\text{PI}} = \lim_{\mu \rightarrow \infty} \lim_{n \rightarrow 0} \lim_{\nu \rightarrow 0} -\frac{1}{M\mu\nu} \ln \left[Z_1^{n-1}(\mu, 0|\mathbf{y}, \mathbf{A}) \int d\boldsymbol{\xi} e^{-\mu\mathcal{H}_1(\boldsymbol{\xi}|\mathbf{y}, \mathbf{A})} \left(\int d_{|\boldsymbol{\xi}|_0} \mathbf{x} e^{-\frac{\mu}{2} \|\mathbf{y} - \mathbf{A}(|\boldsymbol{\xi}|_0 \circ \mathbf{x})\|_2^2} \right)^\nu \right]_{\mathbf{y}, \mathbf{A}} \quad (44)$$

It is now possible to calculate the configurational average by assuming n and ν are natural numbers, and we can follow the usual prescription of the replica method. However, there remains a technical point concerning the limits $n \rightarrow 0$ and $\nu \rightarrow 0$ in the present formulation.

The region around $n = \nu = 0$ has an unusual property. The extremization condition with respect to the order parameters yields several different solutions. Among these solutions, by employing physical arguments [27], we should choose the one analytically connected to $\hat{\Theta}_1$ in (33) in the limit $\nu \rightarrow 0$. This is achieved by the remark given below Eq. (41).

B. Numerical validation using simulations on finite M

1. ℓ_0 -based method

We examine the analytical results, using numerical simulations of finite-size systems. When M is sufficiently small, we can obtain the cumulant-generating function ϕ_0 by exhaustively searching all possible combinations of basis vectors. In cases where M is less small, we use the exchange Monte Carlo (MC) method to sample basis vector combinations obeying the canonical distribution at various temperature points [20], and then estimate the cumulant-generating function ϕ_0 using the multi-histogram method [28].

In all simulations, we set $\alpha = 0.5$ and $\sigma_y^2 = 1$. We treat two values of r equal to 0.2 and 0.4. In the case of $r = 0.2$ (0.4), we calculate cumulant-generating function values at 15 temperature points, which are distributed according to the geometric progression in the range between 1 and 10 (between 1 and 35) in the value of μ . We conduct the exhaustive search for $M \leq 25$ (15), and use the exchange MC method for larger M . The configurational average is calculated by taking the median over 1000 different samples of (\mathbf{y}, \mathbf{A}) . The error bars are estimated by the Bootstrap method.

The procedure for our MC method will now be explained. At every temperature point, we randomly choose the initial vector \mathbf{c} among those satisfying $\|\mathbf{c}\|_0 = rM$. For $r = 0.2$, the number of MC steps required for thermalization and sufficient sampling is 2, 3, 4, 7, 10×10^4 for $M = 30, 35, 40, 45, 50$, respectively, while for $r = 0.4$ it is 2, 4, 8, 15, 30×10^4 for $M = 20, 25, 30, 35, 40$, respectively. The first half of the MC steps are discarded for thermalization. One MC step consists of two parts. First, updating once at every temperature point, and then exchanging once between every pair of neighboring temperature points. In each update of \mathbf{c} , we randomly choose one index i such that $c_i = 1$ and another j such that $c_j = 0$ to flip into the opposite state. That is, we set $c_i = 0$ and $c_j = 1$, and accept or reject this trial according to the Metropolis criterion based on the energy values calculated from \mathcal{H}_0 (12).

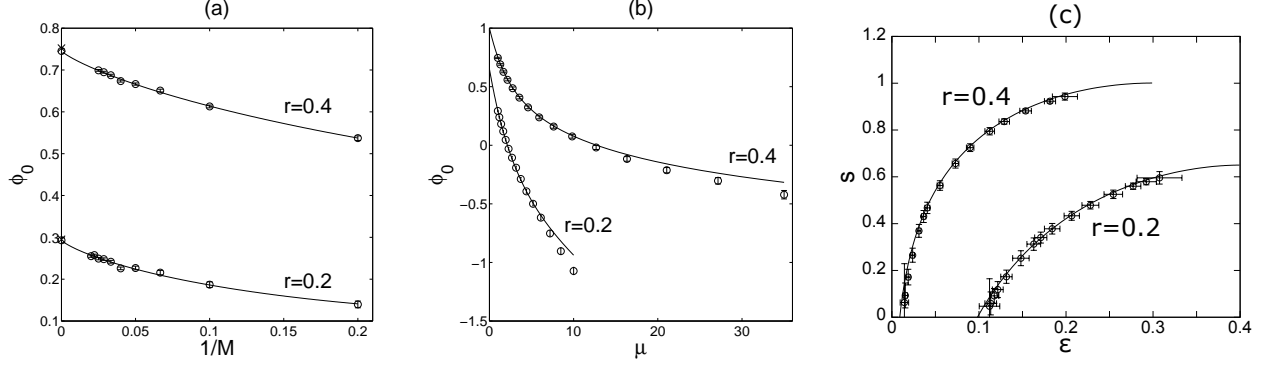


FIG. 3. Cumulant-generating function ϕ_0 and entropy density s of the ℓ_0 -based method with $\sigma_y^2 = 1$, $\alpha = 0.5$, and $r = 0.2, 0.4$. (a) Plots of numerically evaluated ϕ_0 at $\mu = 1$. The lines are given by the linear regression. On the vertical axis, the circles and crosses represent the extrapolated and analytical values in the $M \rightarrow \infty$ limit, respectively. The lengths of the error bars are comparable to the sizes of symbols. (b) Plots of ϕ_0 in the $M \rightarrow \infty$ limit. The lines and circles represent the analytical and extrapolated values, respectively. The lengths of the error bars are comparable to the sizes of symbols. (c) Plots of s against ϵ in the $M \rightarrow \infty$ limit. The lines and circles represent the analytical and extrapolated values, respectively. These are calculated from the values of ϕ_0 in (b).

The Metropolis criterion is also used in the exchange of \mathbf{cs} of different temperature points.

The results of the numerical simulations are presented in Fig. 3. Figure 3(a) shows the results of the cumulant-generating function value at $\mu = 1$. On the vertical axis, the circles represent extrapolated values from finite-size results. The extrapolation lines are given by the linear regression using an asymptotic form $\phi_0 \approx a + bM^{-1} + cM^{-1} \ln M^{-1}$. The regression is conducted by employing the least-squares method, as follows:

$$\min_{a,b,c} \frac{1}{2} \sum_M \left(a + b \frac{1}{M} + c \frac{1}{M} \ln \frac{1}{M} - \phi_0(M) \right)^2. \quad (45)$$

The asymptotic form is based on the Stirling's formula and is exact at $\mu = 0$, which motivates us to use the form even for $\mu \neq 0$. The cumulant-generating function and entropy density in the limit $M \rightarrow \infty$ are presented in Figs. 3(b) and 3(c), respectively. The lines represent the analytical results. The circles represent the extrapolated values from the numerical results. The analytical solutions are seen to be consistent with the numerical ones. Hence, the numerical results clearly validate the analytical results in the ℓ_0 -based method.

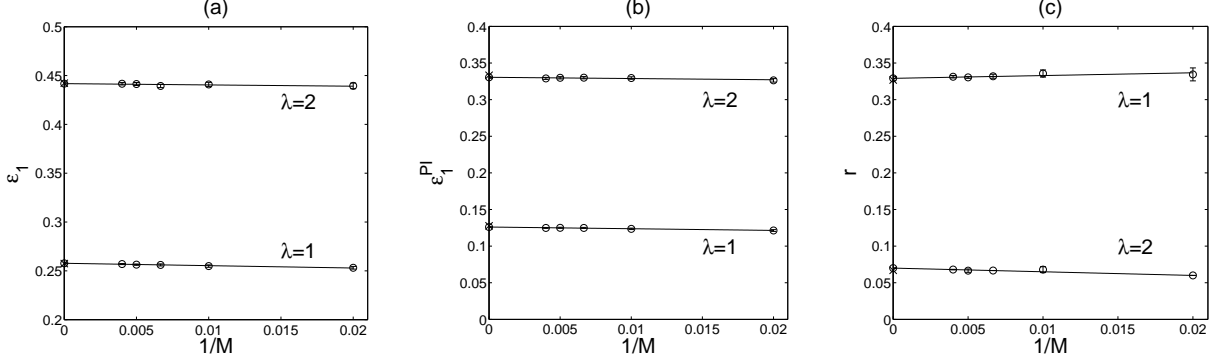


FIG. 4. Plots of numerically evaluated values of the ℓ_1 -based method with $\sigma_y^2 = 1$, $\alpha = 0.5$, and $\lambda = 1, 2$. The extrapolation lines are given by the linear regression. On the vertical axes, the circles and crosses represent the extrapolated and analytical values in the $M \rightarrow \infty$ limit, respectively. The lengths of the error bars are comparable to the sizes of symbols. (a) Reconstruction error before PI, ϵ_1 . (b) Reconstruction error after PI, ϵ_1^{PI} . (c) Reduction rate, r .

2. ℓ_1 -based method

Similarly to the case of the ℓ_0 -based method, we examine the analytical results of the ℓ_1 -based method by performing numerical simulations on finite-size systems. We carry out the ℓ_1 -norm regularization using quadratic programming, and evaluate the error before PI, ϵ_1 ; the error after PI, ϵ_1^{PI} ; and the rate r .

The values of α and σ_y^2 are fixed as $\alpha = 0.5$ and $\sigma_y^2 = 1$ for all simulations. We treat two values of λ equal to 1 and 2. We calculate (9) and (11) using quadratic programming and the PI operation for $M = 50, 100, \dots, 250$.

The results of the numerical simulations are shown in Fig. 4. Figures 4(a)–(c) plot the numerically evaluated error before the PI operation, error after the PI operation, and the rate, respectively, against the system size M . On the vertical axes, the circles and crosses represent extrapolated and analytical values in the $M \rightarrow \infty$ limit, respectively. The extrapolation lines are given by the linear regression using the asymptotic forms $\epsilon_1 \approx a + bM^{-1}$, $\epsilon_1^{\text{PI}} \approx c + dM^{-1}$, and $r \approx e + fM^{-1}$. We see that the analytical solutions are very close to the extrapolated values. This correlation clearly demonstrates the reliability of the analytical results.

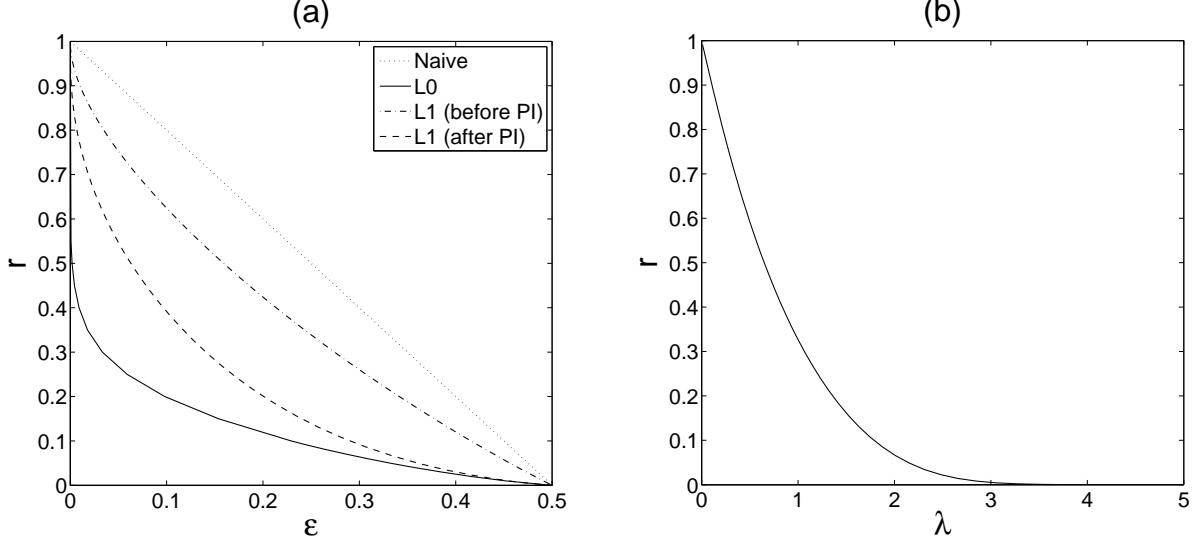


FIG. 5. Results of the analysis in the $M \rightarrow \infty$ limit with $\sigma_y^2 = 1$ and $\alpha = 0.5$. (a) Trade-off relations of the naive, ℓ_0 -based, and ℓ_1 -based methods (before and after the PI operation). (b) Relation between the rate and the regularization coefficient in the ℓ_1 -based method.

C. Comparison in the trade-off relation

We compare the ideal performance in the $M \rightarrow \infty$ limit for different methods in terms of the trade-off relation between the reconstruction error and the reduction rate. Figure 5(a) shows the trade-off relations in the case of $\alpha = 0.5$. We see that both of the OCB-based methods achieve a better trade-off relation than the naive one. In the OCB-based strategy, the ℓ_0 -based method significantly outperforms the ℓ_1 -based one, even if the PI is operated after carrying out the ℓ_1 -norm regularization. We attribute the inferiority of the ℓ_1 -based method to the regularization term. Indeed, as shown in Fig. 5(b), the regularization term is necessary to decrease the rate, but it distorts the original purpose of minimizing the reconstruction error, as clearly seen from Eq. (26).

For a further comparison of the OCB-based methods, Fig. 6 shows the trade-off relations where different values of α control the degree of overcompleteness. Figs. 6(a) and 6(b) present the results of the ℓ_0 - and ℓ_1 -based methods, respectively. In the ℓ_1 -based method, the PI has been operated after the ℓ_1 -norm regularization. Both methods achieve a better trade-off relation as the degree of overcompleteness increases, or α decreases. Another interesting observation is the superiority of the ℓ_0 -based method compared to the ℓ_1 -based one, regardless of the degree of overcompleteness.

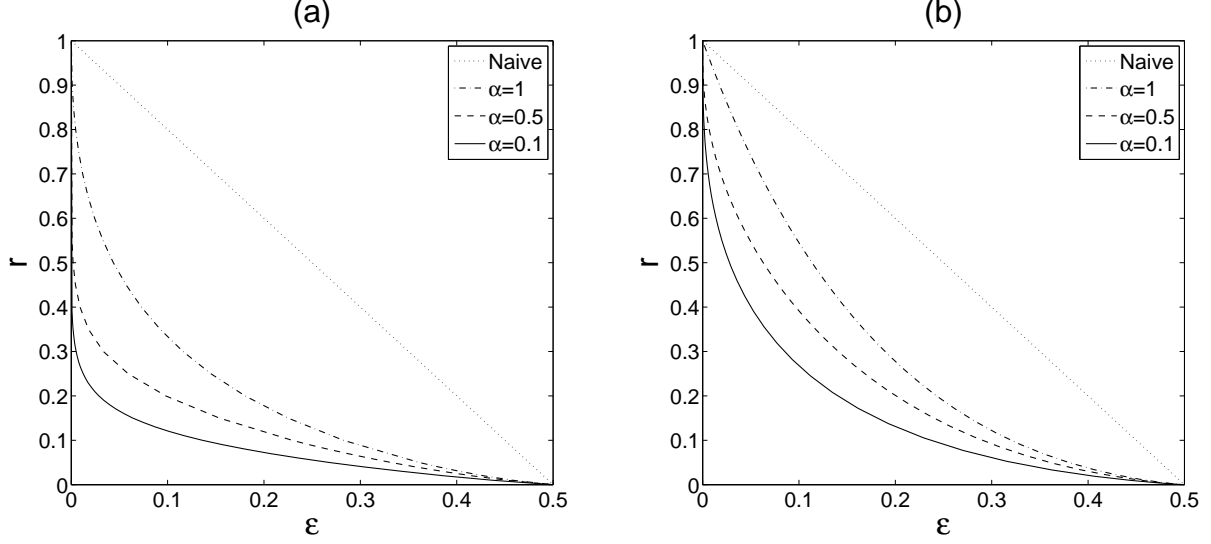


FIG. 6. Trade-off relations at various values of α in the case of $\sigma_y^2 = 1$. (a) Results of the ℓ_0 -based method. (b) Results of the ℓ_1 -based method (after the PI operation). For both the methods, against fixed a r , the reconstruction error ϵ becomes smaller as α decreases.

1. *In the large limit of the degree of overcompleteness, $\alpha \rightarrow 0$*

From Fig. 6 we see that the reconstruction error becomes smaller as α decreases, both for the ℓ_0 - and ℓ_1 -based methods. An interesting question is whether the reconstruction error vanishes or not in the limit $\alpha \rightarrow 0$, or more quantitatively, how ϵ is scaled by α in the small limit.

Deferring the detailed calculations to Appendix A 2 and B 2, here we summarize our analytical results on the behavior of ϵ in the limit $\alpha \rightarrow 0$

$$\epsilon_0 \propto \alpha^{\frac{2r}{1-r}} \rightarrow 0, \quad (46)$$

$$\epsilon_1 \rightarrow \frac{1}{2}(1-r)^2\sigma_y^2 = O(1), \quad (47)$$

$$\epsilon_1^{\text{PI}} \propto |\ln \alpha|^{-1} \rightarrow 0. \quad (48)$$

The asymptotic behaviors of ϵ_0 and ϵ_1^{PI} are examined using numerical solutions of the corresponding EOSs, Eqs. (21,42), in Fig. 7. Our analytic formulas show an excellent agreement with the numerical results.

We stress the consequence of Eqs. (46-48). First, they give a firm indication that it is reasonable to apply the PI after the ℓ_1 -norm regularization, which is heuristically employed in related problems such as compressed sensing in practical situations. The difference in Eqs.

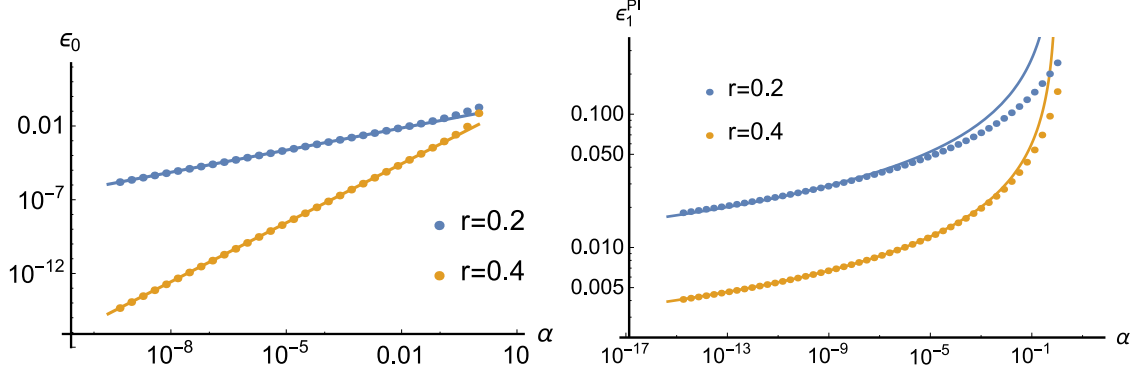


FIG. 7. Plots of ϵ against α in the small α limit, derived by solving Eqs. (21,42) numerically. The left panel represents ϵ_0 , and the right panel represents ϵ_1^{PI} . The lines are the fits based on our analytical formulas, Eqs. (46,48), and these show excellent agreement with the points obtained by the numerical evaluations.

(47,48) indicates that the PI actually diminishes the error, and even eliminates it in the ideal limit $\alpha \rightarrow 0$, which never happens with only the use of ℓ_1 -norm regularization. Second, Eq. (46) provides a general bound for the computational cost of searching the appropriate basis vectors. From Eq. (46), given a target value of the error $\hat{\epsilon}$ and some data on the length M , the required size $N_{\text{req}}(\hat{\epsilon}, M)$ of the basis matrix to achieve this error value is scaled as

$$N_{\text{req}}(\hat{\epsilon}, M) \propto M \hat{\epsilon}^{-\frac{1-r}{2r}}. \quad (\ell_0) \quad (49)$$

This grows in a polynomial manner as the target error value $\hat{\epsilon}$ decreases, and the exponent of the polynomial negatively grows as the reduction rate r decreases. This quantitative information will provide a theoretical basis in designing algorithms. Finally, Eq. (48) manifests the limit of the ℓ_1 -based method. The size N_{req} required to achieve the target error $\hat{\epsilon}$ in this case is scaled as

$$N_{\text{req}}(\hat{\epsilon}, M) \propto M e^{\frac{1}{\hat{\epsilon}}}, \quad (\ell_1 + \text{PI}). \quad (50)$$

This grows exponentially as $\hat{\epsilon}$ decreases, which is considered to be reasonable. If it were a polynomial, versatile algorithms exactly solving the ℓ_1 -norm regularization could be applied to solve the problem with a computational cost of a polynomial order of the system size and the precision, which is believed not to be possible. However, Eq. (50) can still be useful, because it provides a quantitative comparison between the data size M and the acceptable error $\hat{\epsilon}$ in an unified manner.

Input: a data vector \mathbf{y} , a basis matrix \mathbf{A} , a rate r .

Initialization: $\mathbf{x}^{(0)} = \mathbf{0}$, $U = \{1, 2, \dots, N\}$, $S^{(0)} = \emptyset$.

Iteration: repeat from $n = 1$ until $n = rM$:

$$\begin{aligned} \mathbf{r} &= \mathbf{y} - \mathbf{A}\mathbf{x}^{(n-1)}, \\ j &= \arg \max_{k \in U \setminus S^{(n-1)}} \{|\mathbf{a}_k^T \mathbf{r}|\}, \\ S^{(n)} &= S^{(n-1)} \cup \{j\}, \\ \mathbf{x}^{(n)} &= \arg \min_{\mathbf{x}} \{\|\mathbf{y} - \mathbf{A}\mathbf{x}\|_2\} \quad \text{subj. to } \text{supp}(\mathbf{x}) \subset S^{(n)}. \end{aligned}$$

Output: a reduced vector $\hat{\mathbf{x}} = \mathbf{x}^{(rM)}$.

FIG. 8. The procedure of OMP. \emptyset is the empty set. $\text{supp}(\cdot)$ is the support set.

IV. EXAMINATION OF PRACTICAL PERFORMANCE

A. Algorithms and their performances

A lot of computational time is required to conduct the exhaustive search used in for the ℓ_0 -based method. However, it is considered that certain greedy algorithms might work well for practical applications. Orthogonal matching pursuit (OMP, Fig. 8) is a greedy algorithm that may be suitable for the present purpose [21, 22]. OMP only requires a computational time of order $O(M^4)$ for the current purpose. We compare the performance of OMP with the ideal performances of both the ℓ_0 - and ℓ_1 -based methods.

In addition to OMP, we also examine approximate message passing (AMP), as a representative algorithm carrying out the ℓ_1 -norm regularization. From the viewpoint of quadratic programming, ℓ_1 -norm regularization is solved exactly using versatile algorithms, which require a computational time of order $O(M^3)$. In contrast, AMP only requires a computational time of order $O(M^2)$ per update. Despite the low computational cost, AMP is known to be able to recover the results of those versatile algorithms, in certain reasonable situations [23]. The present case, where the basis matrix \mathbf{A} and the data vector \mathbf{y} are generated from i.i.d. normal distributions, is expected to be one such situation. Hence, we can fairly compare the result of AMP with the ideal performance of the ℓ_1 -based method, and therefore with that of OMP.

We evaluate the performances of OMP and AMP when they are employed for dimen-

Input: a data vector \mathbf{y} , a basis matrix \mathbf{A} , a regularization coefficient λ , a tuning parameter δ .

Initialization: $\mathbf{x}^{(0)} = \mathbf{0}$, $\chi^{(0)} = 0$, $\mathbf{r}^{(0)} = \mathbf{y}$.

Iteration: repeat until convergence at $n = \hat{n}$:

$$\begin{aligned}\hat{Q} &= \frac{1}{1+\chi^{(n-1)}}, \\ \mathbf{r}^{(n)} &= (1 - \hat{Q})\mathbf{r}^{(n-1)} + \hat{Q}(\mathbf{y} - \mathbf{A}\mathbf{x}^{(n-1)}), \\ \mathbf{h} &= \mathbf{A}^T \mathbf{r}^{(n)} + \hat{Q}\mathbf{x}^{(n-1)}, \\ \chi^{(n)} &= (1 - \delta)\chi^{(n-1)} + \delta \frac{1}{Q} \frac{1}{M} \sum_i \Theta(|h_i| - \lambda), \\ x_i^{(n)} &= (1 - \delta)x_i^{(n-1)} + \delta \frac{1}{Q} \text{sign}(h_i)(|h_i| - \lambda)\Theta(|h_i| - \lambda) \quad \text{for } i = 1, \dots, N.\end{aligned}$$

Output: a reduced vector $\hat{\mathbf{x}} = \mathbf{x}^{(\hat{n})}$.

FIG. 9. The procedure of AMP. $\text{sign}(\cdot)$ is the sign function. $\Theta(\cdot)$ is the Heaviside step function.

sionality reduction with the OCB-based strategy. We examine the case with $\sigma_y^2 = 1$ and $\alpha = 0.5$. Figure 10 presents the results of the performance evaluations of OMP and AMP. Figure 10(a) shows the results for finite-size systems, namely $M = 50, 100, \dots, 250$, and the extrapolation by the linear regression using an asymptotic form of $\epsilon \approx a + bM^{-1}$. The reduction rate is set to $r = 0.5$ when evaluating OMP, and the regularization coefficient λ is set to 0.65 when evaluating AMP, so that $r \approx 0.5$. We evaluate the performance of AMP based on the reconstruction error after the PI operation. In Fig. 10(b), we compare the extrapolated performances of OMP and AMP at various rates with the achievable trade-off relation analyzed in Sec. III. The AMP result compares well with the ideal performance of the ℓ_1 -based method, while that for OMP does not reach the ideal result of the ℓ_0 -based method. However, a notable finding is that OMP considerably outperforms the ℓ_1 -based results. This motivates the exploration of better algorithms for the ℓ_0 -based method, in the context of the dimensionality reduction. Such exploration is currently under way.

B. Application to image data

We investigate the performance of dimensionality reduction, when it is applied to a task of image data compression. We compress image data composed of 256×256 pixels. The experimental procedure of compression is as follows. First, image data are normalized so as to set the mean and variance to 0 and 1, respectively. Next, 256×256 pixels are randomly

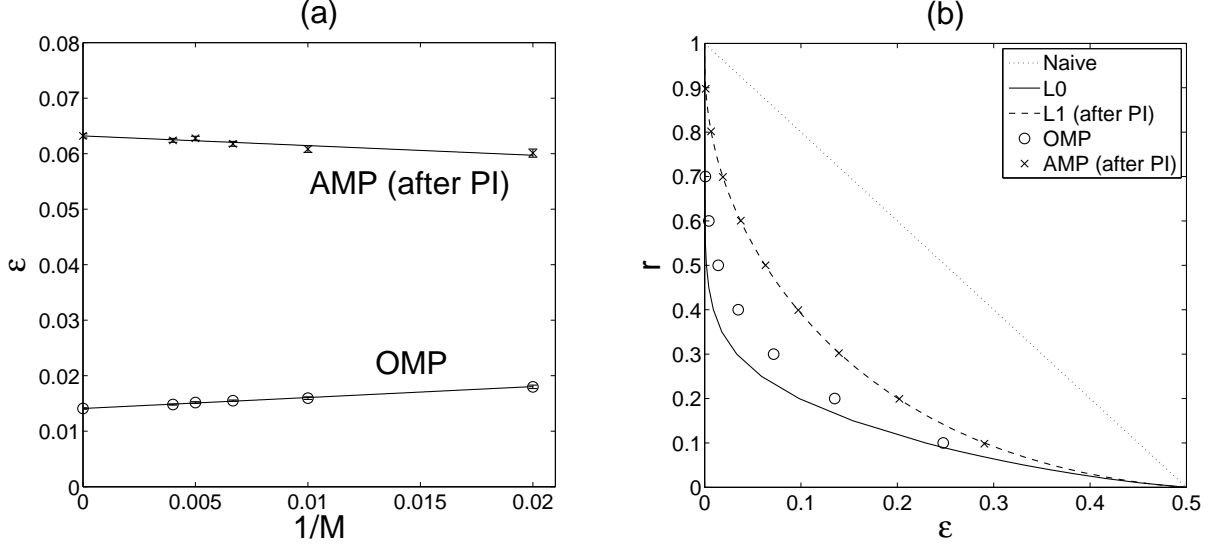


FIG. 10. Performances of OMP and AMP in the case with $\sigma_y^2 = 1$ and $\alpha = 0.5$. The performance of AMP is evaluated after the PI operation. (a) Plots of the numerically evaluated errors in the case of $r = 0.5$. The extrapolation lines are given by the linear regression. On the vertical axis, the symbols represent extrapolated values in the $M \rightarrow \infty$ limit. The lengths of the error bars are comparable to the sizes of symbols. In OMP r is set to $r = 0.5$, and in AMP λ is set to 0.65, so that $r \approx 0.5$. (b) Trade-off relations in the $M \rightarrow \infty$ limit. The circles and crosses represent extrapolated values of OMP and AMP, respectively.

permuted, in order to obtain 1024 column vectors, whose dimensionality is 64. Following these operations, the data can be regarded as random numbers with a mean and variance of 0 and 1, which enables us to compare the data with the theoretical analysis we have already carried out. Finally, setting $r = 0.5$, we compress each of the column vectors into a reduced vector by using a 64×128 random matrix, namely $\alpha = 0.5$. We examine the performances of OMP and AMP. When applying AMP, we set the regularization coefficient to 0.65, so that $r \approx 0.5$, and the PI is operated after carrying out the ℓ_1 -norm regularization. The results of experiments are presented in Fig. 11. Although OMP requires a computational time that is several times larger than that of AMP, OMP outperforms AMP in terms of appearance and peak signal-to-noise ratio (PSNR), defined as

$$\text{PSNR} = 10 \log_{10} \frac{255^2}{\frac{1}{N} \sum_{ij} (\hat{I}_{ij} - I_{ij})^2}, \quad (51)$$

where $\mathbf{I} = \{I_{ij}\}$ and $\hat{\mathbf{I}} = \{\hat{I}_{ij}\}$ represent an original image and a compressed image, respectively, and N is the number of image pixels.

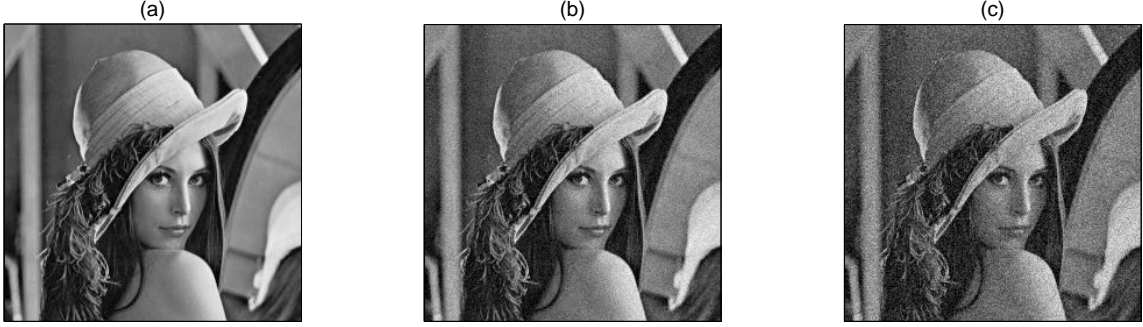


FIG. 11. Application of dimensionality reduction with the OCB-based strategy to image data compression. The degree of overcompleteness is $\alpha = 0.5$. (a) Original image data. (b) Compressed image data recovered from OMP-reduced representation. The reduction rate is $r = 0.5$. PSNR is 28.2. The time required is approximately 55 sec. (c) Compressed image data recovered from the AMP-reduced representation. The regularization coefficient is $\lambda = 0.65$, so that $r \approx 0.5$. The AMP-compressed representation is given after the PI operation. PSNR is 22.9. The time required is approximately 4.5 sec.

If the scope of application is limited to image data compression, more convenient bases, such as a discrete wavelet transformation, will achieve much better results in the performance and computational time [29, 30]. However, in general contexts it is not easy to find a proper basis for compression in advance. A solution to this problem is to use blind compressed sensing and related techniques such as dictionary learning [31–33], but the computational costs are rather high. Our OCB-based strategy may overcome this difficulty, because it avoids the learning of the dictionary by preparing many candidates for basis vectors and choosing a suitable combination. Our theoretical analysis and numerical experiments positively support this possibility.

V. CONCLUSION

In the present paper, sparse-data processing has been discussed from the viewpoint of dimensionality reduction. We have focused on a strategy of dimensionality reduction that is based on an OCB, and have proposed the use of the ℓ_0 - and ℓ_1 -based methods. We have analyzed the ideal performances of these methods in the large-system limit in a statistical-mechanical manner, which has been validated by numerical simulations on finite-size systems

and their extrapolation to the infinite-size limit. Our results have indicated that the ℓ_0 -based method outperforms the naive and ℓ_1 -based methods in terms of the trade-off relation between the reconstruction error and the reduction rate. A notable result is that any small error is achievable for any finite fixed value of the reduction rate, by increasing the degree of overcompleteness, for both the ℓ_0 - and ℓ_1 -based methods. This result allows us to determine both the theoretical limit of the OCB-based strategy and the limit for practical algorithms based on the ℓ_1 regularization. In addition, it provides a firm basis for the use of the pseudoinverse after the ℓ_1 regularization, which is frequently applied in related problems such as compressed sensing in practical situations.

In addition to the ideal performance, we also investigated the practical performance of our strategy. We evaluated the performances of OMP and AMP as algorithms to approximately perform the ℓ_0 - and ℓ_1 -based methods, respectively. Our evaluation showed that OMP surpasses both AMP and the exact execution of the ℓ_1 -based method, in terms of the trade-off relation. This suggests that greedy algorithms are more suitable for dimensionality reduction using our strategy than convex relaxation algorithms, although there is still room to design more effective greedy algorithms than OMP. We are currently undertaking further research in this direction.

We considered the application of our method to image data compression, as a practical example, and evaluated its performance when OMP and AMP are utilized. OMP outperforms AMP in appearance and PSNR, although OMP requires a computational time that is several times larger. In order to efficiently decrease the computational time of our strategy, it is important to find a proper basis. This suggests the use of some prior knowledge in constructing the overcomplete basis. Some further possibilities, such as combining our methods with dictionary learning, are still open, and would be interesting to address in future work.

ACKNOWLEDGMENTS

This work was supported by JSPS KAKENHI Grant Numbers 13J04920 (YN-O), 26870185 (TO), 25120009 (MO), and 25120013 (YK).

Appendix A: Calculations for the ℓ_0 -based method

1. Derivation of ϕ_0

Based on Eq. (25), we define

$$\psi_0(n, \nu, \mu) = \frac{1}{M} \ln \left[\left\{ \text{Tr}_{\mathbf{c}} \left(\int d_{\mathbf{c}} \mathbf{x} e^{-\frac{1}{2\nu} \|\mathbf{y} - \mathbf{A}(\mathbf{c} \circ \mathbf{x})\|_2^2} \right)^\nu \right\}^n \right]_{\mathbf{y}, \mathbf{A}}. \quad (\text{A1})$$

The cumulant-generating function ϕ_0 is recovered from ψ_0 , as $\phi_0(\mu) = \lim_{n, \nu \rightarrow 0} (1/n) \psi_0(n, \nu, \mu)$. When (n, ν) are positive integers, we obtain

$$\psi_0(n, \nu, \mu) = \frac{1}{M} \ln \text{Tr}_{\{\mathbf{c}^a\}} \text{Tr}_{\{\mathbf{x}^{a\alpha}\}} \left[e^{-\frac{\mu}{2\nu} \sum_{j=1}^M \sum_{a=1}^n \sum_{\alpha=1}^\nu (y_j - \sum_i A_{ji} c_i^a x_i^{a\alpha})^2} \right]_{\mathbf{y}, \mathbf{A}}, \quad (\text{A2})$$

where $\text{Tr}_{\{\mathbf{c}^a\}} = \prod_{a=1}^n \sum_{\mathbf{c}^a} \delta(Mr - \sum_i c_i^a)$, and $\text{Tr}_{\{\mathbf{x}^{a\alpha}\}} = \prod_{a=1}^n \prod_{\alpha=1}^\nu \int d_{\mathbf{c}^a} \mathbf{x}^{a\alpha}$. Let us introduce the variables $s_j^{a\alpha} = \sum_i A_{ji} c_i^a x_i^{a\alpha}$ and $Q_{(a\alpha)(b\beta)} = \frac{1}{M} \sum_i (c_i^a x_i^{a\alpha})(c_i^b x_i^{b\beta})$. According to the central limit theorem, we regard the variables $\{s_j^{a\alpha}\}$ as random variables that follow a zero-mean multivariate normal distribution, with covariances $[s_j^{a\alpha} s_k^{b\beta}]_{\mathbf{A}} = \delta_{jk} Q_{(a\alpha)(b\beta)}$. Using these variables, we obtain

$$\psi_0(n, \nu, \mu) = \frac{1}{M} \ln \text{Tr}_{\{\mathbf{c}^a\}} \text{Tr}_{\{\mathbf{x}^{a\alpha}\}} \text{Tr}_{\mathbf{Q}} \left(\left[e^{-\frac{\mu}{2\nu} \sum_a \sum_\alpha (y - s^{a\alpha})^2} \right]_{y, \{s^{a\alpha}\} | \mathbf{Q}} \right)^M, \quad (\text{A3})$$

where $\text{Tr}_{\mathbf{Q}} = \prod_{(a\alpha)(b\beta)} \int dQ_{(a\alpha)(b\beta)} \delta(MQ_{(a\alpha)(b\beta)} - \sum_i (c_i^a x_i^{a\alpha})(c_i^b x_i^{b\beta}))$, and the brackets $[\cdot]_{y, \{s^{a\alpha}\} | \mathbf{Q}}$ denote the average over y and $s^{a\alpha}$, which is conditioned by the variance $Q_{(a\alpha)(b\beta)}$ as explained above.

After introducing the Fourier representation of the delta function, $\delta(\cdot) \propto \int d\tilde{x} e^{\frac{i}{2}(\cdot)}$, the saddle-point method is employed to obtain

$$\begin{aligned} \psi_0(n, \nu, \mu) = \text{extr}_{\Theta_0} & \left\{ \ln \left[e^{-\frac{\mu}{2\nu} \sum_a \sum_\alpha (y - s^{a\alpha})^2} \right]_{y, \{s^{a\alpha}\} | \mathbf{Q}} + \sum_a \frac{\tilde{r}_a}{2} r \right. \\ & \left. + \sum_{(a\alpha)(b\beta)} \frac{\tilde{Q}_{(a\alpha)(b\beta)}}{2} Q_{(a\alpha)(b\beta)} + \frac{1}{\alpha} \ln \sum_{\{\mathbf{c}^a\}} \text{Tr}_{\{\mathbf{x}^{a\alpha}\}} e^{-\sum_a \frac{\tilde{r}_a}{2} c^a - \sum_{(a\alpha)(b\beta)} \frac{\tilde{Q}_{(a\alpha)(b\beta)}}{2} (c^a x^{a\alpha})(c^b x^{b\beta})} \right\}, \quad (\text{A4}) \end{aligned}$$

where $\Theta_0 = \{\mathbf{Q}, \tilde{\mathbf{r}}, \tilde{\mathbf{Q}}\}$. For the extremizer, we search the subspace with $(Q_{(a\alpha)(b\beta)}, \tilde{Q}_{(a\alpha)(b\beta)})$ equal to (Q, \tilde{Q}) ($a = b, \alpha = \beta$), $(q_1, -\tilde{q}_1)$ ($a = b, \alpha \neq \beta$), or $(q_0, -\tilde{q}_0)$ ($a \neq b$), with $\tilde{r}_a = \tilde{r}$. This is the replica symmetry (RS) in the present formula of two replica numbers n and ν .

Then, we obtain

$$\begin{aligned} \psi_0(n, \nu, \mu) = \text{extr}_{\tilde{\Theta}_0} & \left\{ \ln \int Dy Dw \left(\int Dv \left(\int Du e^{-\frac{\mu}{2\nu}(\sigma_y y - \sqrt{q_0} w - \sqrt{q_1 - q_0} v - \sqrt{Q - q_1} u)^2} \right)^\nu \right)^n \right. \\ & + \frac{1}{2} n \tilde{r} r + \frac{1}{2} n \nu \tilde{Q} Q - \frac{1}{2} n \nu (\nu - 1) \tilde{q}_1 q_1 - \frac{1}{2} n (n - 1) \nu^2 \tilde{q}_0 q_0 \\ & \left. + \frac{1}{\alpha} \ln \int Dz \left(\int Dt \sum_c \left(\text{Tr}_{x|c} e^{-\frac{\tilde{r}}{2\nu} c - \frac{\tilde{Q} + \tilde{q}_1}{2} c x^2 + t \sqrt{\tilde{q}_1 - \tilde{q}_0} c x + z \sqrt{\tilde{q}_0} c x} \right)^\nu \right)^n \right\}, \end{aligned} \quad (\text{A5})$$

where $\tilde{\Theta}_0 = \{Q, q_1, q_0, \tilde{r}, \tilde{Q}, \tilde{q}_1, \tilde{q}_0\}$. We assume that Eq. (A5) is true not only for positive integers (n, ν) but also for real numbers (n, ν) . In taking the limits $(n, \nu) \rightarrow (0, 0)$, we introduce $\chi = \beta(Q - q_1)$, $q = q_0$, $\hat{r} = \tilde{r}$, $\hat{Q} = \nu(\tilde{Q} + \tilde{q}_1) - \nu^2 \tilde{q}_1$, $\hat{\chi} = \nu^2 \tilde{q}_1$, and $\hat{q} = \nu^2 \tilde{q}_0$, which are assumed to be of the order $O(1)$ in these limits. Following some straightforward calculations, the replica identity is given by

$$\phi_0(\mu) = \lim_{n, \nu \rightarrow 0} \frac{1}{n} \psi_0(n, \nu, \mu), \quad (\text{A6})$$

thus yielding Eq. (19).

2. The limit $\alpha \rightarrow 0$ in the ℓ_0 case

We examine the behavior of the zero point of entropy, ϵ_0 , in the large-size limit of the basis matrix, $\alpha \rightarrow 0$. The parameter μ corresponding to the zero point ϵ_0 , μ_0 , can be formally written using Eqs. (23,24), as

$$\begin{aligned} \mu_0 = -\frac{\hat{\chi}(\mu_0)}{2\phi_0(\mu_0)} = -\frac{1}{2} \hat{\chi} & \left\{ \frac{1}{2} \ln \frac{1 + \chi}{1 + \chi + \mu_0 \Delta} - \frac{1}{2} \frac{\mu_0(q + \sigma_y^2)}{1 + \chi + \mu_0 \Delta} \right. \\ & \left. + \frac{1}{2} \left(\hat{r} r + \hat{Q} Q - \frac{\hat{\chi}}{\mu_0} \chi + \hat{q} q \right) + \frac{1}{\alpha} \int Dz \ln \left(1 + \sqrt{\frac{\hat{\chi} + \hat{Q}}{\hat{Q} + \hat{q}}} e^{-\frac{1}{2} \hat{r} + \frac{1}{2} \frac{\hat{q}}{\hat{Q} + \hat{q}} z^2} \right) \right\}^{-1}. \end{aligned} \quad (\text{A7})$$

A numerical calculation indicates the behavior of $\mu_0 \rightarrow \infty$ as $\alpha \rightarrow 0$, while $\hat{Q}, \hat{q}, Q, q, \chi \sim O(1)$ are kept finite. We will determine the scalings of the relevant variables for $\alpha \rightarrow 0$ so as to agree with these observations. A crucial observation from Eq. (21d) is that the factor Y should vanish, in order to cancel the vanishing α , yielding

$$\frac{1}{\alpha} Y \propto \frac{\sqrt{\mu_0}}{\alpha} e^{-\frac{1}{2} \hat{r}} = O(1) \Rightarrow \begin{cases} \hat{r} = \tilde{r} - 2\rho \ln \alpha \\ \mu_0 \propto \alpha^{2-2\rho} \end{cases}, \quad (\text{A8})$$

where we introduce an exponent ρ controlling the divergence speed of \hat{r} and μ_0 . Since we assume the divergence of μ_0 , ρ must be larger than unity. The value of ρ is determined by solving Eq. (A7) in a self-consistent manner. The scaling of the remaining order parameter $\hat{\chi}$ is determined by

$$\hat{\chi} \rightarrow \frac{\mu_0(\alpha)}{1+\chi} + \frac{q+\sigma_y^2}{\Delta^2} \rightarrow \infty. \quad (\text{A9})$$

Now, we know all of the scalings of the order parameters, and can reduce Eq. (A7) to the dominant part, as

$$\mu_0 \approx \frac{\frac{\mu_0}{1+\chi} + \frac{q+\sigma_y^2}{\Delta^2}}{2\rho r \ln \alpha + \ln(1+\chi+\mu_0\Delta)}. \quad (\text{A10})$$

By solving this in the leading scaling, we obtain

$$\rho = \frac{1}{1-r}, \quad \mu_0 \approx \frac{e^{(1+\chi)^{-1}}}{\Delta} \alpha^{-2\frac{r}{1-r}} + O(1). \quad (\text{A11})$$

By inserting Eqs. (A9,A11) into Eq. (23), we get Eq. (46)

Appendix B: Some calculations for the ℓ_1 -based methods

1. Derivations of f_1 and ϵ_1^{PI}

Based on Eq. (44), we introduce

$$\psi_1(n, \nu, \beta, \mu, \kappa) = \frac{1}{M} \ln \left[Z_1^{n-1}(\mu, \kappa | \mathbf{y}, \mathbf{A}) \int d\boldsymbol{\xi} e^{-\mu(\mathcal{H}_1(\boldsymbol{\xi} | \mathbf{y}, \mathbf{A}) + \kappa \|\boldsymbol{\xi}\|_0)} \left(\int d|_{\boldsymbol{\xi}|_0} \mathbf{x} e^{-\frac{\beta}{2} \|\mathbf{y} - \mathbf{A}(|_{\boldsymbol{\xi}|_0} \mathbf{x})\|_2^2} \right)^\nu \right]_{\mathbf{y}, \mathbf{A}} \quad (\text{B1})$$

By calculating this in the case of positive integers (n, ν) , we obtain

$$\psi_1(n, \nu, \beta, \mu, \kappa) = \frac{1}{M} \ln \text{Tr}_{\{\boldsymbol{\xi}^a\}} \text{Tr}_{\{\mathbf{x}^\alpha\}} \left(\left[e^{-\frac{\mu}{2} \sum_a (y_j - \sum_i A_{ji} \xi_i^a)^2 - \frac{\beta}{2} \sum_a (y_j - \sum_i A_{ji} |\xi_i^a|_0 x_i^\alpha)^2} \right]_{\mathbf{y}, \mathbf{A}} \right)^M, \quad (\text{B2})$$

where $\text{Tr}_{\{\boldsymbol{\xi}^a\}} = \prod_{a=1}^n \int d\boldsymbol{\xi}^a e^{-\mu(\lambda \sum_i |\xi_i^a| + \kappa \sum_i |\xi_i^a|_0)}$, and $\text{Tr}_{\{\mathbf{x}^\alpha\}} = \prod_{\alpha=1}^\nu \int d|_{\boldsymbol{\xi}^1|_0} \mathbf{x}^\alpha$. Let us introduce the variables $s_j'^a = \sum_i A_{ji} \xi_i^a$, $s_j^\alpha = \sum_i A_{ji} |\xi_i^1|_0 x_i^\alpha$, $P_{ab} = \frac{1}{M} \sum_i \xi_i^a \xi_i^b$, $C'_{a\alpha} = \frac{1}{M} \sum_i \xi_i^a (|\xi_i^1|_0 x_i^\alpha)$, $C_{\alpha a} = \frac{1}{M} \sum_i (|\xi_i^1|_0 x_i^\alpha) \xi_i^a$, and $Q_{\alpha\beta} = \frac{1}{M} \sum_i (|\xi_i^1|_0 x_i^\alpha) (|\xi_i^1|_0 x_i^\beta)$. As in the ℓ_0 case, we can rewrite the variables $\{s_j'^a, s_j^\alpha\}$ as random variables from a zero-mean multivariate normal distribution, with the covariances $[s_j'^a s_k'^b]_{\mathbf{A}} = \delta_{jk} P_{ab}$, $[s_j'^a s_k^\alpha]_{\mathbf{A}} = \delta_{jk} C_{a\alpha}$, $[s_j'^\alpha s_k^a]_{\mathbf{A}} = \delta_{jk} C'_{a\alpha}$, and $[s_j^\alpha s_k^\beta]_{\mathbf{A}} = \delta_{jk} Q_{\alpha\beta}$. Using these variables, we obtain

$$\begin{aligned} & \psi_1(n, \nu, \beta, \mu, \kappa) \\ &= \frac{1}{M} \ln \text{Tr}_{\{\boldsymbol{\xi}^a\}} \text{Tr}_{\{\mathbf{x}^\alpha\}} \text{Tr}_{\mathbf{P}} \text{Tr}_{\mathbf{C}} \text{Tr}_{\mathbf{C}'} \text{Tr}_{\mathbf{Q}} \left(\left[e^{-\frac{\mu}{2} \sum_a (y_j - s_j'^a)^2 - \frac{\beta}{2} \sum_a (y_j - s_j^\alpha)^2} \right]_{y_j, \{s_j'^a, s_j^\alpha\} | \mathbf{P}, \mathbf{C}, \mathbf{C}', \mathbf{Q}} \right)^M, \quad (\text{B3}) \end{aligned}$$

where $\text{Tr}_{\mathbf{P}} = \prod_{a,b} \int dP_{ab} \delta(MP_{ab} - \sum_i \xi_i^a \xi_i^b)$, $\text{Tr}_{\mathbf{C}} = \prod_{a,\alpha} \int dC_{a\alpha} \delta(MC_{a\alpha} - \sum_i (|\xi_i^1|_0 x_i^\alpha) \xi_i^a)$, $\text{Tr}_{\mathbf{C}'} = \prod_{a,\alpha} \int dC'_{a\alpha} \delta(MC'_{a\alpha} - \sum_i \xi_i^a (|\xi_i^1|_0 x_i^\alpha))$, and $\text{Tr}_{\mathbf{Q}} = \prod_{\alpha,\beta} \int dQ_{\alpha\beta} \delta(MQ_{\alpha\beta} - \sum_i (|\xi_i^1|_0 x_i^\alpha) (|\xi_i^1|_0 x_i^\beta))$. After introducing the Fourier representation of the delta function, the saddle-point method is employed, to obtain

$$\begin{aligned} \psi_1(n, \nu, \beta, \mu, \kappa) = & \text{extr}_{\Theta_1} \left\{ \ln \left[e^{-\frac{\mu}{2} \sum_a (y-s'^a)^2 - \frac{\beta}{2} \sum_\alpha (y-s^\alpha)^2} \right]_{y, \{s'^a, s^\alpha\} | \mathbf{P}, \mathbf{C}, \mathbf{C}', \mathbf{Q}} \right. \\ & + \sum_{a,b} \frac{\tilde{P}_{ab}}{2} P_{ab} + \sum_{a,\alpha} \frac{\tilde{C}_{a\alpha}}{2} C_{a\alpha} + \sum_{\alpha,a} \frac{\tilde{C}'_{\alpha a}}{2} C'_{\alpha a} + \sum_{\alpha,\beta} \frac{\tilde{Q}_{\alpha\beta}}{2} Q_{\alpha\beta} \\ & \left. + \frac{1}{\alpha} \ln \text{Tr}_{\{\xi^a\}} \text{Tr}_{\{x^\alpha\}} e^{-\sum_{a,b} \frac{\tilde{P}_{ab}}{2} \xi^a \xi^b - \sum_{a,\alpha} \frac{\tilde{C}_{a\alpha} + \tilde{C}'_{\alpha a}}{2} \xi^a (|\xi^1|_0 x^\alpha) - \sum_{\alpha,\beta} \frac{\tilde{Q}_{\alpha\beta}}{2} (|\xi^1|_0 x^\alpha) (|\xi^1|_0 x^\beta)} \right\}, \quad (\text{B4}) \end{aligned}$$

where $\Theta_1 = \{\mathbf{P}, \mathbf{C}, \mathbf{C}', \mathbf{Q}, \tilde{\mathbf{P}}, \tilde{\mathbf{C}}, \tilde{\mathbf{C}'}, \tilde{\mathbf{Q}}\}$. For the extremizer, we search the subspace with (P_{ab}, \tilde{P}_{ab}) equal to (P, \tilde{P}) ($a = b$) or $(p, -\tilde{p})$ ($a \neq b$); $(C_{a\alpha}, \tilde{C}_{a\alpha})$ equal to $(C'_{\alpha a}, \tilde{C}'_{\alpha a}) = (C, -\tilde{C})$ ($a = 1$) or $(c, -\tilde{c})$ ($a \neq 1$); and $(Q_{\alpha\beta}, \tilde{Q}_{\alpha\beta})$ equal to (Q, \tilde{Q}) ($\alpha = \beta$) or $(q, -\tilde{q})$ ($\alpha \neq \beta$). This is the RS assumption for the present case. Thus, we obtain

$$\begin{aligned} \psi_1(n, \nu, \beta, \mu, \kappa) = & \text{extr}_{\tilde{\Theta}_1^{\text{PI}}, \tilde{\Theta}_1} \left\{ \ln \int Dy Dz Dw \left(\int Dv e^{-\frac{\mu}{2} (\sigma_y y - \sqrt{p}w - \sqrt{P-p}v)^2} \right)^{n-1} \right. \\ & \times \int Dv e^{-\frac{\mu}{2} (\sigma_y y - \sqrt{p}w - \sqrt{P-p}v)^2} \left(\int Du e^{-\frac{\beta}{2} (\sigma_y y - \frac{c}{\sqrt{p}}w - \frac{C-c}{\sqrt{P-p}}v - \sqrt{q - \frac{(C-c)^2}{P-p} - \frac{c^2}{p}}z - \sqrt{Q-qu})^2} \right)^\nu \\ & + \frac{1}{2} n \tilde{P} P - \frac{1}{2} n(n-1) \tilde{p} p - \nu \tilde{C} C - (n-1) \nu \tilde{c} c + \frac{1}{2} \nu \tilde{Q} Q - \frac{1}{2} \nu(\nu-1) \tilde{q} q \\ & + \frac{1}{\alpha} \ln \int Dz Dw Dv Du \left(\text{Tr}_\xi e^{-\frac{\tilde{P}+\tilde{p}}{2} \xi^2 + (u\sqrt{p-\tilde{c}}+v\sqrt{\tilde{c}})\xi} \right)^{n-1} \\ & \times \text{Tr}_\xi e^{-\frac{\tilde{P}+\tilde{p}+\tilde{C}-\tilde{c}}{2} \xi^2 + (u\sqrt{p-\tilde{c}}+w\sqrt{\tilde{C}-\tilde{c}+v\sqrt{\tilde{c}}})\xi} \\ & \left. \times \left(\text{Tr}_x e^{-\frac{\tilde{Q}+\tilde{q}+\tilde{C}-\tilde{c}}{2} (|\xi|_0 x)^2 + (z\sqrt{\tilde{q}-\tilde{c}}+w\sqrt{\tilde{C}-\tilde{c}+v\sqrt{\tilde{c}}})|\xi|_0 x} \right)^\nu \right\}, \quad (\text{B5}) \end{aligned}$$

where $\tilde{\Theta}_1^{\text{PI}} = \{C, c, Q, q, \tilde{C}, \tilde{c}, \tilde{Q}, \tilde{q}\}$ and $\tilde{\Theta}_1 = \{P, p, \tilde{P}, \tilde{p}\}$.

The free-energy density f_1 is now derived as

$$f_1(\mu, \kappa) = - \lim_{n \rightarrow 0} \lim_{\nu \rightarrow 0} \frac{1}{\mu n} \psi_1(n, \nu, \beta, \mu, \kappa) \quad (\text{B6})$$

$$\begin{aligned} = & \text{extr}_{\tilde{\Theta}_1} \left\{ \frac{1}{2\mu} \ln(1 + \mu(P-p)) + \frac{1}{2} \frac{P + \sigma_y^2}{1 + \mu(P-p)} - \frac{1}{2\mu} (\tilde{P}P + \tilde{p}p) \right. \\ & \left. - \frac{1}{\mu\alpha} \int Dv \ln \text{Tr}_\xi e^{-\frac{\tilde{P}+\tilde{p}}{2} \xi^2 + v\sqrt{\tilde{p}}\xi} \right\}. \quad (\text{B7}) \end{aligned}$$

In the limit $\mu \rightarrow \infty$, we introduce $\chi_p = \mu(P - p)$, $\hat{P} = \mu^{-1}(\tilde{P} + \tilde{p})$, and $\hat{\chi}_p = \mu^{-2}\tilde{p}$, which are assumed to be of the order $O(1)$. Taking the $\mu \rightarrow \infty$ limit in Eq. (B7) leads to Eq. (33).

On the other hand, in order to evaluate ϵ_1^{PI} , in addition to $\hat{\Theta}_1 = P, \chi_p, \hat{P}, \hat{\chi}_p$, in taking the limit $\mu \rightarrow \infty$ we define the parameters $\chi_c = \beta(C - c)$, $\chi_q = \beta(Q - q)$, $\hat{C} = \beta^{-1}(\tilde{C} + \tilde{c})$, $\hat{\chi}_c = \beta^{-2}\tilde{c}$, $\hat{Q} = \beta^{-1}(\tilde{Q} + \tilde{q})$, and $\hat{\chi}_q = \beta^{-2}\tilde{q}$, which are assumed to be of the order $O(1)$. Then, through the formula

$$\epsilon_1^{\text{PI}} = \lim_{\mu \rightarrow \infty} \lim_{n \rightarrow 0} \lim_{\nu \rightarrow 0} \frac{1}{\nu} \psi_1(n, \nu, \mu, \mu, 0), \quad (\text{B8})$$

we obtain Eq. (41).

2. The limit $\alpha \rightarrow 0$ in the ℓ_1 case

The EOSs (34) show that in the limit $\alpha \rightarrow 0$ we have

$$\chi_p, \hat{P}, \hat{\chi}_p = O(1). \quad (\text{B9})$$

From Eq. (35) and the asymptotic formula of the complementary error function $\text{erfc}(\cdot)$, we see in the limit $\alpha \rightarrow 0$ we have

$$\frac{e^{-\frac{1}{2}\theta^2}}{\alpha\sqrt{2\pi}\theta} = O(1), \Rightarrow \theta = O(\sqrt{|\ln \alpha|}) \rightarrow \infty, \quad (\text{B10})$$

which is realized by controlling λ as $O(\sqrt{|\ln \alpha|})$. Using these scalings, and the asymptotic expansion of the complementary error function for large θ in Eq. (34d), we obtain

$$P = O(\theta^{-2}) = O(|\ln \alpha|^{-1}) \rightarrow 0. \quad (\text{B11})$$

By inserting these scalings into Eq. (37), we obtain Eq. (47).

The asymptotic form of ϵ_1^{PI} can be similarly obtained. Following some lengthy but

straightforward calculations, we obtain

$$\hat{\chi}_q = O(|\ln \alpha|^{-1}) \rightarrow 0, \quad (\text{B12a})$$

$$\hat{Q} = O(1), \quad (\text{B12b})$$

$$\hat{\chi}_c = O(|\ln \alpha|^{-1}) \rightarrow 0, \quad (\text{B12c})$$

$$\hat{C} = O(1), \quad (\text{B12d})$$

$$\chi_q = O(1), \quad (\text{B12e})$$

$$Q = O(|\ln \alpha|^{-1}) \rightarrow 0, \quad (\text{B12f})$$

$$\chi_c = O(1), \quad (\text{B12g})$$

$$C = O(|\ln \alpha|^{-1}) \rightarrow 0. \quad (\text{B12h})$$

By substituting these scalings into Eq. (43c), we obtain Eq. (48).

-
- [1] K. Pearson, *Philosophical Magazine*, **2**(11), 559–572 (1901).
 - [2] C. Eckart and G. Young, *Psychometrika*, **1**(3), 211–218 (1936).
 - [3] X. Su and T.M. Khoshgoftaar, *Advances in Artificial Intelligence*, **2009**, 421425 (2009).
 - [4] I. Markovsky, *Low Rank Approximation: Algorithms, Implementation, Applications*, Springer, London (2012).
 - [5] B.A. Olshausen and D.J. Field, *Nature*, **381**, 607–609 (1996).
 - [6] B.A. Olshausen and D.J. Field, *Vision Research*, **37**(23), 3311–3325 (1997).
 - [7] B.A. Olshausen and D.J. Field, *Current Opinion in Neurobiology*, **14**(4), 481–487 (2004).
 - [8] H. Terashima and H. Hosoya, *Network: Computation in Neural Systems*, **20**(4), 253–267 (2009).
 - [9] H. Terashima and M. Okada, in *Advances in Neural Information Processing System 25*, 2312–2320 (2012).
 - [10] H. Terashima, H. Hosoya, T. Tani, N. Ichinohe and M. Okada, *Neurocomputing*, **103**(1), 14–21 (2013).
 - [11] D.L. Donoho, *IEEE Transactions on Information Theory*, **52**(4), 1289–1306 (2006).
 - [12] E.J. Candès and T. Tao, *IEEE Transactions on Information Theory*, **51**(12), 4203–4215 (2005).

- [13] E.J. Candès, J. Romberg and T. Tao, *IEEE Transactions on Information Theory*, **52**(2), 489–509 (2006).
- [14] E.J. Candès and T. Tao, *IEEE Transactions on Information Theory*, **52**(12), 5406–5425 (2006).
- [15] S.T. Roweis and L.K. Saul, *Science*, **290**, 2323–2326 (2000).
- [16] E. Bingham and H. Mannila, in *Proceedings of the seventh ACM SIGKDD international conference on Knowledge discovery and data mining*, 245–250 (2001).
- [17] S. Foucart and H. Rauhut, *A Mathematical Introduction to Compressive Sensing*, Springer, Berlin (2013).
- [18] H. Nishimori, *Statistical Physics of Spin Glasses and Information Processing: An Introduction*, Oxford University Press, Oxford (2001).
- [19] V. Dotsenko, *Introduction to the replica theory of disordered statistical systems*, Cambridge University Press, New York (2001).
- [20] K. Hukushima and K. Nemoto, *Journal of the Physical Society of Japan*, **65**, 1604–1608 (1996).
- [21] S. Chen, S.A. Billings and W. Luo, *International Journal of Control*, **50**(5), 1873–1896 (1989).
- [22] Y.C. Pati, R. Rezaeiifar and P.S. Krishnaprasad, *1993 Conference Record of The Twenty-Seventh Asilomar Conference on Signals, Systems and Computers*, 40–44 (1993).
- [23] D.L. Donoho, A. Maleki and A. Montanari, *Proceedings of the National Academy of Sciences*, **106**(45), 18914–18919 (2009).
- [24] R. Monasson and D. O’Kane, *Europhysics Letters*, **27**(2), 85–90 (1994).
- [25] R. Tibshirani, *Journal of the Royal Statistical Society: Series B (Methodological)*, **58**(1), 267–288 (1996).
- [26] We have an additional comment for readers familiar with spin-glass theory. Our present framework in calculating ϕ_0 is actually similar to the one-step replica-symmetry-breaking (1RSB) ansatz. In this identification, ν is identified as the 1RSB breaking parameter (usually written as m), and each configuration of \mathbf{c} corresponds to a pure state in the 1RSB free-energy landscape; the entropy can be regarded as complexity.
- [27] This technique for handling Eq. (44) is very similar to the so-called Franz-Parisi potential in spin-glass theory. This is a versatile tool to calculate a probabilistic model conditioned by another probabilistic model. For interested readers, we refer to S. Franz and G. Parisi, *Physical Review Letters*, **79**, 2486 (1997).

- [28] A.M. Ferrenberg and R.H. Swendsen, *Physical Review Letters*, **61**(23), 2635–2638 (1988).
- [29] A. Skodras, C. Christopoulos and T. Ebrahimi, *IEEE Signal Processing Magazine*, **18**(5), 36–58 (2001).
- [30] E.J. Candès and M.B. Wakin, *IEEE Signal Processing Magazine*, **25**(2), 21–30 (2008).
- [31] R. Rubinstein, A.M. Bruckstein and M. Elad, *Proceedings of the IEEE*, **98**(6), 1045–1057 (2010).
- [32] S. Gleichman and Y.C. Eldar, *IEEE Transactions on Information Theory*, **57**(10), 6958–6975 (2011).
- [33] A. Sakata and Y. Kabashima, *Europhysics Letters*, **103**, 28008-p1–28008-p6 (2013).